Journal of Sound and Vibration 492 (2021) 115770

Contents lists available at ScienceDirect

Journal of Sound and Vibration

journal homepage: www.elsevier.com/locate/jsv

A semi-analytical solution for acoustic wave propagation in varying area ducts with mean flow

Saikumar R. Yeddula*, Aimee S. Morgans

Department of Mechanical Engineering, Imperial College London, London, UK

ARTICLE INFO

Article history:
Received 6 March 2020
Revised 30 September 2020
Accepted 2 October 2020
Available online 3 October 2020

Keywords:
Semi-analytical solution
WKB method
Linearised Euler equations
Acoustic-entropy coupling

ABSTRACT

A semi-analytical solution is developed for the propagation of plane acoustic waves in a varying area duct, sustaining a 1-D mean flow with a temperature gradient. The mean flow can be non-isentropic, such that the axial variation of the flow area and temperature can be prescribed independently. The case of an isentropic mean flow, for which the flow area and mean temperature variation are linked, is discussed. A second order differential equation (ODE) for acoustic pressure is derived from the linearised Euler equations in the frequency domain, neglecting the communication between acoustic and entropy disturbances. This ODE has axially varying coefficients and is solved using an iterative WKB approximation method. The obtained wave-like solution is expressed as the superposition of downstream and upstream propagating plane wave amplitudes. The solution thus obtained is, at any location, a function of upstream thermodynamic and mean-flow properties and wave-number, and can be applied to ducts with arbitrarily varying area and temperature profiles. For validation of the model, two shapes of area variation with linear temperature gradient are considered, and the solution is further simplified to depend only on local spatial coordinate and inlet conditions. The semi-analytical solutions are valid at "high" frequencies, thus the frequencies considered must be both low enough for a predominantly one-dimensional acoustic field, and large enough for validity of the solutions. For each geometry, the analytical solution is presented along with the frequency range of its validity. The analytical predictions are compared to numerical solutions of the linearised Euler equations (LEEs), which can either account for or neglect the acoustic - entropy wave coupling; this further allows the coupling effect to be evaluated. Within the frequency ranges of their validity, the simplified semi-analytical solutions perform well up to flow Mach-numbers around 0.3. For inlet temperature fluctuations $\sim 1\%$ of the mean, the effect of acoustic-entropy coupling on the accuracy analytical prediction was found to be insignificant for flow Mach numbers less than 0.3.

1. Introduction

Thermoacoustic instabilities, also known as combustion instabilities, occur due to a two-way coupling between unsteady heat release and acoustics. If acoustic pressure fluctuations are in-phase with unsteady heat release rate at the flame, and

* Corresponding author.
E-mail addresses: s.yeddula18@imperial.ac.uk (S.R. Yeddula), a.morgans@imperial.ac.uk (A.S. Morgans).

https://doi.org/10.1016/j.jsv.2020.115770

if the resulting energy gain of perturbations exceeds the acoustic energy flux leaving the control volume [1], the amplitude of acoustic oscillations grows. This causes high levels of noise and system vibration until the effects of acoustic nonlinearities leads to limit-cycling or other non-linear oscillations. Thermoacoustic instabilities are highly undesirable. They are also difficult to simulate, the disparity between the acoustic length scales, which are O(metre), and the flame wrinkling, O(millimetre), and flame reactions O(micrometre), making it very computationally costly.

Computational methods which couple separate treatments for the acoustic waves and the flame have been shown to have much promise for accurate prediction [2–11]. A model for the unsteady flame response to acoustic excitation can be extracted from large eddy simulations [9,11–20], while the acoustic waves can be treated using low order network modelling [8,9,21–29] or Helmholtz solvers [10,30–33]. Of particular motivation for this work are low order network models, these implementing analytical solutions for the acoustic field in simple geometry "modules" which are then networked together. For duct modules with uniform cross-sectional area and mean flow, it is straightforward for analytical models to account for mean flow effects. However, for ducts which exhibit spatial gradients in the mean flow, temperature and cross-sectional area, current network models either discretise the duct into connected segments each with uniform flow [34,35], or are limited to specific simple cases. It is beneficial for network models to represent the acoustic field as a superposition of upstream and downstream propagating acoustic wave components, this offering physical insight, facilitating connection to other modules and enabling acoustic damping estimates for any attached dampers. Analytical solutions offer the benefits of guaranteed convergence, irrespective of grid size, make parametric studies much easier and are therefore helpful in identifying efficient ways of altering the system to attenuate thermo-acoustic oscillations during the design stage.

Analytical solutions for the one-dimensional acoustic field in a duct of varying area are broadly divided into exact solutions and semi-analytical solutions. Exact analytical solutions for a subsonic nozzle flow were firstly derived for acoustically compact geometries by Marble and Candel [36]. The acoustic wavelength was considered significantly larger than the length scale of the nozzle area-change, such that nozzle appears as a 'step' to the incident acoustic wave. Eisenberg and Kao [37], determined the acoustic solution for an isentropic flow without temperature gradients using transformation techniques for specific area profiles, leading to ordinary differential equations with constant coefficients. For incompressible, isentropic mean flows with very low Mach numbers, ($M^2 < < 1$), Easwaran and Munjal [38] presented exact solutions and corresponding transfer matrices for conical and exponential duct area profiles. For uniform area ducts with linear temperature gradient, Munjal and Prasad [39] derived the acoustic transfer matrix using perturbation theory. Other exact solutions for low subsonic mean flow in uniform ducts with temperature gradient include [40,41]. Exact traveling wave-type solutions for specific area and temperature profiles were obtained for non-uniform ducts with mean-temperature gradient and negligible mean flow by Subrahmanyam and Sujith [42]. An exact solution for acoustic wave propagation in a varying area duct for the general case - with both substantial mean-flow and a temperature gradient, has not been possible. For this reason, semi-analytical solutions came into prominence, these combining good accuracy with high computational efficiency.

The WKB approximate method, named after Wentzel, Kramers, and Brillouin [43], is a technique traditionally used in wave-mechanics to obtain approximate wave-like solutions for second order differential equations with variable coefficients. Though this method predates the method of multiple scales, it works in a similar manner. It essentially assumes that the phase varies more rapidly than the amplitude of the wave, requiring a high frequency assumption.

Cummings [44] used a slightly modified WKB method with separate amplitude and phase factors instead of an asymptotic expansion. This led to an analytical solution for the acoustic field in a varying area duct with very low Mach number, isentropic mean-flow and no entropy perturbations, valid at high frequencies. This approach was extended to ducts of constant cross-sectional area, sustaining a practical non-isentropic mean flow with a temperature gradient by Li and Morgans [45]. The final solution included integrals of rapidly varying phase, leading to higher computational time compared to an analytical solution. Dokumaci [46] presented a semi-analytical solution for a varying area duct with non-zero isentropic mean flow. This was derived by retaining only the off-diagonal terms in the state-space matrix for the isentropic flow equations. The limiting frequency criteria were derived for zero mean flow. The model performs well over a slightly narrower frequency range than WKB-based models, and requires marginally more computational effort [47] as the terms in the state-space matrix are integrated over the domain (the solution depends on the thermodynamic and flow properties in the entire region). Rani and Rani [48] presents approximate (WKB and WKB2) solutions to the acoustic field in quasi 1-D varying area ducts with inhomogeneous mean flow properties, but the analysis was again restricted to isentropic flows. The WKB solution achieved consists of complicated parameters, making the solution computationally costly, and unclear of the frequency limits. Hence there remains a gap for WKB-based models which apply to non-isentropic mean flows and which are only a function of local thermodynamic and flow properties.

For non-isentropic mean flows, Umurhan [49] studied the effect of different spatial heating distributions, with no heat release fluctuations, on thermoacoustic stability. Dokumaci [50] presented numerical solutions to the 1-D linearised Euler equations for non-isentropic mean flows, further discussing the conditions for the isentropic formulation to apply, and when the entropy (error) wave is not negligible.

Semi-analytical solutions derived from truncation of an infinite series have also been used to determine the acoustic field. For example, Duran and Moreau [51] used a Magnus expansion to solve for the acoustic field in a varying area duct sustaining an isentropic mean flow. In order to apply the Magnus expansion, the Euler equations were recast in terms of flow invariants - mass, stagnation temperature and entropy fluctuations in the low frequency limit. This method does not express the final solution as independent plane wave amplitudes; applying the boundary conditions is then not straightforward. It cannot be extended to non-isentropic mean flows, as this would not allow entropy to be considered a flow invariant.

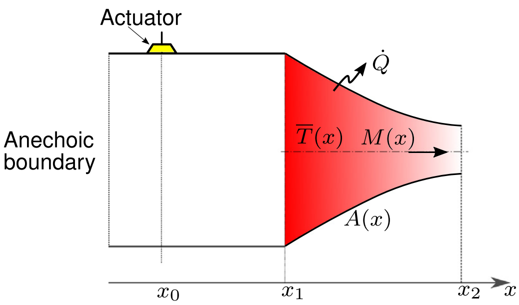

Fig. 1. Sketch of a duct with varying cross-sectional area (x_1 to x_2). $A(x)$, $M(x)$, and $\overline{T}(x)$ represent the duct cross-sectional area, flow Mach number and mean-temperature for given x. For the validation test cases, actuation upstream of the area variation, and an anechoic boundary upstream of actuation are considered.

The main contribution of the present work is to derive a semi-analytical solution for the 1-D acoustic field in a duct which (i) has a varying cross-sectional area, (ii) sustains a non-negligible subsonic mean flow, which may be non-isentropic and (iii) exhibits a streamwise temperature variation, as shown diagrammatically in Fig. 1. A solution will be derived using the WKB-method for the first time, considering firstly non-isentropic duct flows, in which the axial temperature and area gradients can be prescribed independently. The solution for isentropic duct flows, in which the axial temperature and area gradients are inter-related, is also presented.

The analysis assumes that the wave fronts are far enough from their source that they behave as planar 1-D waves, with the acoustic field then depending only on the coordinate in the direction of propagation. The frequencies are assumed sufficiently large that WKB methods can be used, yet sufficiently low that higher-order acoustic modes are not cut-on. A two step procedure is adopted. Firstly, a new differential equation in terms of only acoustic pressure is derived for the first time for non-isentropic mean flows. This differential equation is then solved using an iterative WKB method for the acoustic field. Terms with flow Mach number of order $O(M^3)$ and higher are neglected - a reasonable assumption for combustors and after-burners which require low Mach number flows, typically around 0.2, to keep the flame attached.

Further sections are organized as follows. For non-isentropic flows, the derivation of the acoustic wave equation and its analytical solution using a modified WKB approximation technique are presented in Section 2. The frequency limits of the method, terminology for transfer functions, and validation against linearised Euler equations numerical results are presented for both conical and exponential nozzle geometries. The results for isentropic flows are then presented in Section 3, along with corresponding frequency limits. In Section 4, the effect of acoustic-entropy coupling on the accuracy of the analytical solution is evaluated by comparing with simulations of the linearised Euler equations which account for acoustic-entropy coupling. Conclusions are drawn in the final Section.

2. Non-isentropic varying area flows

In practice, non-isentropic mean flow effects are likely to have a strong bearing on the acoustic field. For example, heat losses from the walls of a combustor cause a mean temperature drop, which will affect the acoustic field. The conservation equations for one-dimensional perfect inviscid flow in a duct with a changing cross-sectional area along with mean temperature variation are,

- **Mass conservation**

$$A\frac{\partial \rho}{\partial t} + \frac{\partial(\rho A u)}{\partial x} = 0 \tag{1}$$

- **Momentum conservation**

$$\frac{\partial u}{\partial t} + u\frac{\partial u}{\partial x} + \frac{1}{\rho}\frac{\partial p}{\partial x} = 0 \tag{2}$$

- **Energy conservation and equation of state**

$$\frac{\partial s}{\partial t} + u\frac{\partial s}{\partial x} = \frac{R_g}{p}\dot{Q} \quad \text{and} \quad p = \rho R_g T \tag{3, 4}$$

where ρ, p, T, u, s, R_g, denote density, pressure, temperature, axial velocity, entropy and universal gas-constant respectively. Based on the principle of linearization, all flow variables can be separated into a mean time-averaged component, denoted by $\bar{(\,)}$, and a perturbation component, denoted by $(\,)'$. The net heat interaction to the surroundings, $\bar{\dot{Q}}$, is not zero for non-isentropic flow. It is also assumed that there are no heat fluctuations inside the duct ($\dot{Q}' = 0$). Further, in this analysis R_g and γ (the ratio of the specific heats), are assumed to be constants with values of 287 J kg^{-1} K^{-1} and 1.4 respectively.

The linearised equations thus obtained are converted from the time to the frequency domain by assuming a time-dependence of the form $y' = \hat{y}e^{i\omega t}$, where ω represents the complex angular frequency and $i = \sqrt{-1}$, as follows,

$$\left(\mathrm{i}\omega + \gamma^2 M^2 \tfrac{\mathrm{d}\bar{u}}{\mathrm{d}x} + \tfrac{1}{\bar{T}}\tfrac{\mathrm{d}\bar{T}}{\mathrm{d}x}\gamma\bar{u}\right)\hat{p} + \bar{u}\tfrac{\mathrm{d}\hat{p}}{\mathrm{d}x} + \left(\tfrac{\mathrm{d}\bar{p}}{\mathrm{d}x}\left(\tfrac{1}{M^2} + 1 - \gamma\right) + \gamma\bar{p}\tfrac{1}{\bar{T}}\tfrac{\mathrm{d}\bar{T}}{\mathrm{d}x}\right)\hat{u} + \gamma\bar{p}\tfrac{\mathrm{d}\hat{u}}{\mathrm{d}x} = 0, \tag{5}$$

$$\left(\mathrm{i}\omega + \frac{\mathrm{d}\bar{u}}{\mathrm{d}x}\right)\hat{u} + \bar{u}\frac{\mathrm{d}\hat{u}}{\mathrm{d}x} + \bar{u}\frac{\mathrm{d}\bar{u}}{\mathrm{d}x}\frac{\hat{p}}{\gamma\bar{p}} + \frac{1}{\bar{\rho}}\frac{\mathrm{d}\hat{p}}{\mathrm{d}x} = \bar{u}\cancelto{\sim 0}{\frac{\mathrm{d}\bar{u}}{\mathrm{d}x}}\hat{\sigma}, \tag{6}$$

$$\mathrm{i}\omega\hat{\sigma} + \bar{u}\frac{\mathrm{d}\hat{\sigma}}{\mathrm{d}x} = \bar{u}\left(\frac{\alpha M^2(\gamma-1)) - \beta\left(1 - M^2\right)}{1 - \gamma M^2}\right)\left(\frac{\hat{u}}{\bar{u}} + \frac{\hat{p}}{\bar{p}}\right). \tag{7}$$

where $\hat{\sigma} = \hat{s}/c_p$ and $c_p = \gamma R_g/(\gamma - 1)$. In the above equations, thermodynamic relations are used to replace the density perturbation, $\hat{\rho}$, with pressure, $\hat{p}$, and normalised entropy, $\hat{\sigma}$, perturbations, as given by,

$$\hat{\sigma} = \frac{\hat{p}}{\gamma\bar{p}} - \frac{\hat{\rho}}{\bar{\rho}}. \tag{8}$$

The communication between the entropy and the acoustic field, as implied by the right hand side of the momentum equation in Eq. (6), is neglected in this analysis. That is, acoustic-entropy coupling is neglected, the justification being that the flow Mach number is low [46,52]. Also, the current analysis is aimed at mid to high frequencies, where the wavelength of entropy disturbances, given as $\bar{u}/f$, is smaller than the largest turbulent length scales. As the entropy wave advects along the duct, its amplitude is then strongly attenuated due to shear dispersion [53–56].

The validity of neglecting acoustic-entropy coupling is further investigated in Section 4, by comparing the analytical results with numerical solution of Eqs. (5)–(7), accounting for acoustic-entropy coupling. A lower value of normalised entropy fluctuation (~ 1%) is considered for this investigation due to higher shear dispersion at these frequencies. In this work, numerical simulations of the linearised Euler equations in which acoustic-entropy coupling is neglected are referred to as 2LEEs (two linearised Euler equations), while simulations which account for it are referred to as 3LEEs (three linearised Euler equations).

For the duct flow, the area and mean-temperature gradients are normalised according to:

$$\alpha = \frac{1}{A}\frac{\mathrm{d}A}{\mathrm{d}x}; \qquad \beta = \frac{1}{\bar{T}}\frac{\mathrm{d}\bar{T}}{\mathrm{d}x}. \tag{9, 10}$$

The mean heat-transfer rate expressed in terms of mean flow gradients as,

$$\bar{\dot{Q}} = \bar{\rho}\,\bar{u}\left(c_p\frac{\mathrm{d}\bar{T}}{\mathrm{d}x} + \bar{u}\frac{\mathrm{d}\bar{u}}{\mathrm{d}x}\right). \tag{11}$$

The steady components of the conservation equations (Eqs. (1)–(3)) allow various mean flow gradients to be expressed in terms of α and β as,

$$\frac{1}{\bar{u}}\frac{\mathrm{d}\bar{u}}{\mathrm{d}x} = \frac{\beta - \alpha}{1 - \gamma M^2}; \ \frac{1}{\bar{p}}\frac{\mathrm{d}\bar{p}}{\mathrm{d}x} = \frac{-\gamma M^2(\beta - \alpha)}{1 - \gamma M^2}; \ \frac{1}{\bar{\rho}}\frac{\mathrm{d}\bar{\rho}}{\mathrm{d}x} = \frac{-\left(\beta - \alpha\gamma M^2\right)}{1 - \gamma M^2}; \ \frac{1}{\bar{c}}\frac{\mathrm{d}\bar{c}}{\mathrm{d}x} = \frac{\beta}{2}. \tag{12 – 15}$$

For non-isentropic flows, the energy equation, Eq. (7), has a source term that depends on temperature and area gradients. This implies that the magnitude of the entropy disturbance can vary as it is transported.

On dividing Eq. (5) by $\gamma\bar{p}$, and Eq. (6) by $\bar{u}$, coefficients of $\mathrm{d}\hat{u}/\mathrm{d}x$ are normalized, and the equations become,

$$A\hat{p} + B\frac{\mathrm{d}\hat{p}}{\mathrm{d}x} + C\hat{u} + \frac{\mathrm{d}\hat{u}}{\mathrm{d}x} = 0; \qquad D\hat{p} + E\frac{\mathrm{d}\hat{p}}{\mathrm{d}x} + F\hat{u} + \frac{\mathrm{d}\hat{u}}{\mathrm{d}x} \approx 0, \tag{16, 17}$$

where the coefficients A, B, C, D, E, F, are functions of x and wavenumber, $k_o = \omega/\bar{c}$, and are given by,

$$A = \frac{1}{\bar{\rho}\bar{c}}\left(\mathrm{i}k_o + \gamma^2 M^2\frac{1}{\bar{u}}\frac{\mathrm{d}\bar{u}}{\mathrm{d}x} + \gamma\beta\right),\ B = \frac{\bar{u}}{\gamma\bar{p}},\ C = \frac{1}{\gamma\bar{p}}\left(\frac{\mathrm{d}\bar{p}}{\mathrm{d}x}\left(\frac{1}{M^2} + 1 - \gamma\right) + \beta\right),$$

$$D = \frac{1}{\gamma\bar{p}}\frac{\mathrm{d}\bar{u}}{\mathrm{d}x},\ E = \frac{1}{\bar{\rho}\bar{u}},\ F = \frac{\mathrm{i}k_o}{M} + \frac{1}{\bar{u}}\frac{\mathrm{d}\bar{u}}{\mathrm{d}x}. \tag{18a–f}$$

Equations (16) and (17) are used to eliminate $\mathrm{d}\hat{u}/\mathrm{d}x$, so that $\hat{u}$ is expressed in terms of $\hat{p}$ and $\mathrm{d}\hat{p}/\mathrm{d}x$ as,

$$\hat{u} = G\hat{p} + H\frac{\mathrm{d}\hat{p}}{\mathrm{d}x}; \quad \text{where } G = \left(\frac{D - A}{C - F}\right) \text{ and } H = \left(\frac{E - B}{C - F}\right). \tag{19}$$

Eq. (19) and its differential with respect to x then replace $\hat{u}$ and $\mathrm{d}\hat{u}/\mathrm{d}x$ in Eq. (16)), leading to a second order differential equation (ODE) in $\hat{p}$:

$$H\frac{\mathrm{d}^2\hat{p}}{\mathrm{d}x^2} + \left(G + \frac{\mathrm{d}H}{\mathrm{d}x} + CH + B\right)\frac{\mathrm{d}\hat{p}}{\mathrm{d}x} + \left(CG + \frac{\mathrm{d}G}{\mathrm{d}x} + A\right)\hat{p} = 0. \tag{20}$$

Upon using relations from Eqs. (12)–(15) and (18a–f), the coefficients of the second order differential equation are simplified. Further assuming β is of the order α and defining $\delta \sim \frac{O(\alpha)}{k_o}$ or $\frac{O(\beta)}{k_o}$, $\kappa = \frac{1}{\alpha^2}\frac{d\alpha}{dx} \sim O(1)$, the ODE takes the following form upon neglecting terms of order δ^3 and M^3 and higher:

$$\begin{aligned}
&\left(1-M^2+\overbrace{(\beta-2\alpha)\frac{iM}{k_o}}^{O(\delta M)}-\overbrace{(\beta-2\alpha)^2\frac{M^2}{k_o^2}}^{O(\delta^2 M^2)}\right)\frac{d^2\hat{p}}{dx^2}\\
-k_o&\left(2iM-\overbrace{\frac{\alpha+\beta}{k_o}}^{O(\delta)}+\overbrace{\frac{\alpha M^2(1+\gamma)+\beta M^2}{k_o}}^{O(\delta M^2)}-\overbrace{\frac{2i\beta(\beta-2\alpha)M}{k_o^2}-\frac{iM}{k_o^2}\left(\frac{d\beta}{dx}-2\frac{d\alpha}{dx}\right)}^{O(\delta^2 M)}\right)\frac{d\hat{p}}{dx}\\
+{k_o}^2&\left(1-\overbrace{\frac{i\beta M}{k_o}(1+\gamma)}^{O(\delta M)}+\overbrace{\frac{3\alpha^2M^2}{k_o^2}\left(1-\frac{1}{\alpha^2}\frac{d\alpha}{dx}\right)-\frac{\alpha\beta M^2}{k_o^2}(8-\gamma)+\frac{\beta^2M^2}{k_o^2}(2-\gamma)\left(2+\frac{1}{\beta^2}\frac{d\beta}{dx}\right)}^{O(\delta^2 M^2)}\right)\hat{p}=0.
\end{aligned} \tag{21}$$

This is the differential equation for the acoustic pressure disturbance in a varying-area duct with an arbitrary temperature gradient and non-isentropic mean flow. The main assumptions underpinning it are: (*i*) the acoustic field is one-dimensional, (*ii*) $|\delta| < < 1$ and $\kappa \sim O(1)$, (*iii*) constant gas properties γ, R_g, (*iv*) weak acoustic-entropy coupling and (*v*) low Mach number, such that terms of $O(M^3)$ and higher are negligible. The coefficients of this ODE are functions only of spatial coordinate, x, and wave-number, k_o. The ODE simplifies to better-known forms under more restrictive assumptions:

- When the mean-flow is negligible ($M \approx 0$), Eq. (21) simplifies to:

$$\frac{d^2\hat{p}}{dx^2}-(\alpha+\beta)\frac{d\hat{p}}{dx}+{k_o}^2\hat{p}=0, \tag{22}$$

consistent with [42].
- For a straight duct without mean-temperature variation ($\alpha = 0,\ \beta = 0$) but sustaining a mean flow, Eq. (21) simplifies to:

$$\left(1-M^2\right)\frac{d^2\hat{p}}{dx^2}-2iMk_o\frac{d\hat{p}}{dx}+{k_o}^2\hat{p}=0. \tag{23}$$

This is consistent with the forms in Ingard and Singhal [57], Lieuwen [59].
- For a straight duct ($\alpha = 0$) with zero mean-temperature gradient ($\beta = 0$) and negligible mean flow ($M \approx 0$), Eq. (21) simplifies to the classic one-dimensional Helmholtz equation [60]:

$$\frac{d^2\hat{p}}{dx^2}+{k_o}^2\hat{p}=0. \tag{24}$$

2.1. Semi-analytical solution using an iterative WKB method

The iterative WKB technique used by Li and Morgans [45] is now applied to the varying-area duct with non-isentropic mean flow. It involves expressing the pressure perturbation as,

$$\hat{p}(x,\omega)=I\exp\int_{x_1}^{x}\left(a^{\pm}(x^*)+ib^{\pm}(x^*)\right)dx^* \tag{25}$$

where, I is an arbitrary constant and a and b are two real x-dependant variables determined using the ODE in Eq. (21). b represents the rapidly varying phase of the wave, while a is related to the slowly varying amplitude, and hence it is assumed that $b \gg a$. The pressure solution can be represented in terms of independent upstream and downstream propagating plane wave amplitudes at high frequencies, where the length scale of the area change sufficiently exceeds the acoustic wavelength. In thermoacoustics, the imaginary part of the wave-number, k_o, is typically much smaller than the real part [8,9,58,59] for modes of interest, and hence the former is neglected for the WKB analysis (when calculating the modes of the conical duct with isentropic mean flow considered in this analysis (shown on the left of Fig. 2), this assumption led to minor errors in growth rate only at the lowest frequency fundamental mode (error ~ 10%) while other modes are accurately captured (error <1%) compared to [29]). In the final solution however, k_o is still regarded complex such that it can be used for stability analysis.

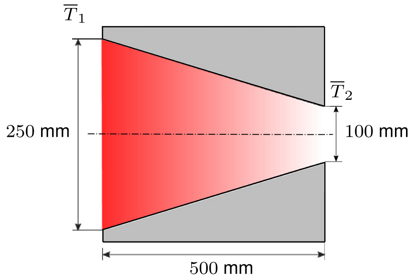

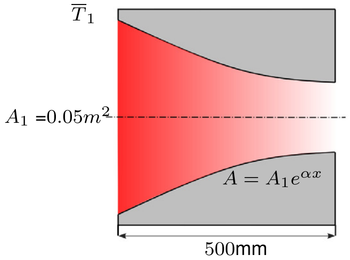

	Inlet	Outlet
$M = \frac{\overline{u}}{\overline{c}}$	0.05	0.27
$\lvert\alpha\rvert$	2.5	6
$\overline{T}$	1600K	1200K
$\overline{c}$	802ms^{-1}	694s^{-1}
$f^*_{high} = \frac{0.293\overline{c}_x}{r_x}$	1880Hz	4693Hz
He^*_{high}	1.2	2.9
f^*_{low}, from Eq. (60)	128Hz	470Hz
He^*_{low}	0.08	0.3

	Inlet	Outlet
$M = \frac{\overline{u}}{\overline{c}}$	0.06	0.28
$\lvert\alpha\rvert$	3	3
$\overline{T}$	1600K	1200K
$\overline{c}$	802ms^{-1}	694ms^{-1}
$f^*_{high} = \frac{0.293\overline{c}_x}{r_x}$	1864Hz	3882Hz
He^*_{high}	1.2	2.4
f^*_{low}, from Eq. (76)	237Hz	257Hz
He^*_{low}	0.15	0.16

Fig. 2. (Left) Schematic of the conical-shaped duct with the flow parameters and calculated frequency limits for non-isentropic mean flow. (Right) Schematic of the exponential-shaped duct with the flow parameters and calculated frequency limits for non-isentropic mean flow. (Frequency limits, corresponding Helmholtz numbers based on length of the duct and mean speed of sound at inlet ($He = fl/\bar{c}_1$) are also presented.).

Substituting Eq. (25) into Eq. (21) gives,

$$\begin{aligned}
&\left(1 - M^2 + \overbrace{(\beta - 2\alpha)\frac{\mathrm{i}M}{k_o}}^{\mathrm{O}(\delta M)} - \overbrace{(\beta - 2\alpha)^2\frac{M^2}{k_o^2}}^{\mathrm{O}(\delta^2 M^2)}\right)\left(a^2 - b^2 + \mathrm{i}2ab + \tfrac{\mathrm{d}a}{\mathrm{d}x} + \mathrm{i}\tfrac{\mathrm{d}b}{\mathrm{d}x}\right)\\
&-k_o\left(2\mathrm{i}M - \overbrace{\frac{\alpha+\beta}{k_o}}^{\mathrm{O}(\delta)} + \overbrace{\frac{\alpha M^2(1+\gamma)+\beta M^2}{k_o}}^{\mathrm{O}(\delta M^2)} - \overbrace{\frac{2\mathrm{i}\beta(\beta-2\alpha)M}{k_o^2} - \frac{\mathrm{i}M}{k_o^2}\left(\frac{\mathrm{d}\beta}{\mathrm{d}x} - 2\frac{\mathrm{d}\alpha}{\mathrm{d}x}\right)}^{\mathrm{O}(\delta^2 M)}\right)(a+\mathrm{i}b)\\
&+{k_o}^2\left(1 - \overbrace{\frac{\mathrm{i}\beta M}{k_o}(1+\gamma)}^{\mathrm{O}(\delta M)} + \overbrace{\frac{3\alpha^2 M^2}{k_o^2}\left(1 - \frac{1}{\alpha^2}\frac{\mathrm{d}\alpha}{\mathrm{d}x}\right) - \frac{\alpha\beta M^2}{k_o^2}(8-\gamma) + \frac{\beta^2 M^2}{k_o^2}(2-\gamma)\left(2 + \frac{1}{\beta^2}\frac{\mathrm{d}\beta}{\mathrm{d}x}\right)}^{\mathrm{O}(\delta^2 M^2)}\right) = 0.
\end{aligned} \tag{26}$$

An iterative procedure is adopted to determine the values of a and b. The initial value of a, denoted a_0, is set to that for the case of negligible mean flow; $a_0^{\pm} = -\frac{\alpha}{2} - \frac{\beta}{4}$, hence a is of the order, $a \sim \mathrm{O}(\alpha)$ or $\mathrm{O}(\beta)$ [44]. Also, the variable b, with initial value b_0, is of the order k_o and so $\frac{b_0}{k_o} \sim \mathrm{O}(1)$.

Now on equating the real part of Eq. (26) to zero, dividing by k_o^2,

$$
\begin{aligned}
&1-\tfrac{b_0^2}{k_o^2}\left(1-M^2\right)+2M\tfrac{b_0}{k_o}+\overbrace{\frac{1}{k_o^2}\left(a_0^2+a_0(\alpha+\beta)+\frac{\mathrm{d}a_0}{\mathrm{d}x}\right)}^{\textbf{Terms 1 - }\ \mathrm{O}(\delta^2)}-\overbrace{\frac{M}{k_o^3}\left(\left(2ab_0+\frac{\mathrm{d}b_0}{\mathrm{d}x}+2b_0\beta\right)(\beta-2\alpha)+b_0\left(\frac{\mathrm{d}\beta}{\mathrm{d}x}-2\frac{\mathrm{d}\alpha}{\mathrm{d}x}\right)\right)}^{\textbf{Terms 2 - }\ \mathrm{O}(\delta^2 M)}\\
&-\overbrace{\frac{M^2}{k_o^2}\left(a_0^2+a_0(\alpha(1+\gamma)+\beta)+\frac{\mathrm{d}a_0}{\mathrm{d}x}-\frac{b_0^2}{k_o^2}(\beta-2\alpha)^2-3\left(\alpha^2-\frac{\mathrm{d}\alpha}{\mathrm{d}x}\right)+\alpha\beta(8-\gamma)-(2-\gamma)\left(2\beta^2+\frac{\mathrm{d}\beta}{\mathrm{d}x}\right)\right)}^{\textbf{Terms 3 - }\ \mathrm{O}(\delta^2 M^2)}\\
&-\overbrace{\frac{(\beta-2\alpha)^2M^2}{k_o^4}\left(a_0^2+\frac{da_0}{dx}\right)}^{\textbf{Terms 4 - }\ \mathrm{O}(\delta^4 M^2)}=0.
\end{aligned}
\tag{27}
$$

Although the WKB method requires the frequency to be large, the frequency must also be small enough for higher order acoustic duct modes to remain cut-off. Thus, a heuristic lower frequency limit above which the WKB approximate solution is valid is discussed, along with an upper frequency limit based on the cut-off criterion. These frequency limits are presented in detail in Section 2.2.

As for any multi-scale method, the WKB method has parameters at different scales. In the current problem, b represents the rapidly varying phase of the wave like solution, while a is of the order of the area gradient, representing the slowly varying amplitude. Under a high frequency approximation, b is of the order k_o, and hence is much larger than a. Hence in Eq. (27), Terms 3 & 4 can be dropped as they are of order $\mathrm{O}(\delta^2M^2)$ and higher. Further, for the first iteration, as $|\delta|$ is considered much smaller than 1, Terms 1, 2 which are of order $\mathrm{O}(\delta^2)$ and $\mathrm{O}(\delta^2M)$ respectively, can also be neglected (these are considered in the second iteration). These assumptions leads to the quadratic equation given by,

$$
1-\frac{b^2}{k_o^2}\left(1-M^2\right)+2M\frac{b}{k_o}\approx 0.
\tag{28}
$$

Solutions for the above equation yield updated values of b:

$$
{b_1}^{\pm}=\frac{\mp k_o}{1\pm M}.
\tag{29}
$$

Similarly on equating the imaginary part of Eq. (26) to zero,

$$
\begin{aligned}
&\overbrace{\frac{2ab_1}{k_o^2}+\frac{1}{k_o^2}\frac{\mathrm{d}b_1}{\mathrm{d}x}+\frac{b_1(\alpha+\beta)}{k_o^2}}^{\textbf{Terms 1 - }\ \mathrm{O}(\delta)}-\overbrace{M\left(\frac{b_1^2(\beta-2\alpha)}{k_o^3}+\frac{2a}{k_o}+\frac{\beta(1+\gamma)}{k_o}\right)}^{\textbf{Terms 2 - }\ \mathrm{O}(\delta M)}\overbrace{-M^2\left(\frac{2ab_1}{k_o^2}+\frac{1}{k_o^2}\frac{\mathrm{d}b_1}{\mathrm{d}x}+\frac{b_1\alpha(1+\gamma)}{k_o^2}+\frac{b_1\beta}{k_o^2}\right)}^{\textbf{Terms 3 - }\ \mathrm{O}(\delta M^2)}\\
&\overbrace{+M\left(\frac{a^2}{k_o^2}\frac{(\beta-2\alpha)}{k_o}+\frac{1}{k_o^2}\frac{\mathrm{d}a}{\mathrm{d}x}\frac{(\beta-2\alpha)}{k_o}+\frac{2a}{k_o}\frac{\beta(\beta-2\alpha)}{k_o^2}+\frac{a}{k_o}\frac{1}{k_o^2}\left(\frac{\mathrm{d}\beta}{\mathrm{d}x}-\frac{\mathrm{d}\alpha}{\mathrm{d}x}\right)\right)}^{\textbf{Terms 4 - }\ \mathrm{O}(\delta^3 M)}\overbrace{-M^2\tfrac{(\beta-2\alpha)^2}{k_o^2}\left(\frac{2ab_1}{k_o^2}+\frac{1}{k_o^2}\frac{\mathrm{d}b_1}{\mathrm{d}x}\right)}^{\textbf{Terms 5 - }\ \mathrm{O}(\delta^3 M^2)}=0,
\end{aligned}
\tag{30}
$$

we obtain an equation whose leading order term is $\mathrm{O}(\delta)$. Neglecting terms of order $\mathrm{O}(\delta^3M)$ and higher, and solving for $a^{\pm}$ results in,

$$
a^{\pm}=\overbrace{-\frac{\alpha}{2}-\frac{\beta}{4}}^{\textbf{Terms }1}\mp\overbrace{\left(\frac{\beta}{2}-\alpha\right)M+\left(\frac{\beta}{2}-\alpha\right)M^2}^{\textbf{Terms }2}+\overbrace{\frac{\alpha\gamma M^2}{2}\mp\frac{\beta\gamma M}{2}}^{\textbf{Terms }3}+\cancelto{0}{\mathrm{O}(\alpha M^3,\beta M^3)}.
\tag{31}
$$

The solution for $a^{\pm}$ as given in Eq. (31), leads to updates for $b^{\pm}$ by again solving the quadratic equation in Eq. (27) and considering terms of order up to $\mathrm{O}(\delta^2M)$ (Terms 1 and 2 included),

$$
\frac{b^{\pm}}{k_o}=\frac{M\mp\sqrt{1-\frac{\Phi_{NI}^{\pm}(1-M^2)}{k_o^2}}}{1-M^2}+O\left(\delta^2M^2\right),
\tag{32}
$$

where $\Phi_{NI}^{\pm}$ is given by,

$$
\begin{aligned}
\tfrac{\Phi_{NI}^{\pm}}{k_o^2}=\ &-\tfrac{1}{k_o^2}\left((a^{\pm})^2+a^{\pm}(\alpha+\beta)+\tfrac{da^{\pm}}{dx}\right)-\tfrac{M}{k_o^3}\left(\left(2a^{\pm}b^{\pm}+\tfrac{db^{\pm}}{dx}+2b^{\pm}\beta\right)(\beta-2\alpha)+b^{\pm}\left(\tfrac{d\beta}{dx}-2\tfrac{d\alpha}{dx}\right)\right)+O\left(\delta^2M^2\right)\\
=\ &\tfrac{1}{k_o^2}\left[\tfrac{\alpha^2}{4}+\tfrac{3\beta^2}{16}+\tfrac{\alpha\beta}{2}\mp M\left(\alpha^2+\tfrac{\beta^2}{2}(1-\gamma)-\tfrac{\alpha\beta}{2}(3-\gamma)\right)+\tfrac{d\alpha}{dx}\left(\tfrac{1}{2}\pm M\right)+\tfrac{1}{2}\tfrac{d\beta}{dx}\left(\tfrac{1}{2}\pm M(\gamma-1)\right)\right].
\end{aligned}
\tag{33}
$$

For $\frac{\Phi^{\pm}_{NI}}{k_o^2}$, which is of the order δ^2 ($|\delta| \ll 1$), the binomial expansion can be applied to Eq. (32); retaining terms up to first order gives,

$$\frac{b^{\pm}}{k_o} = \frac{\mp 1}{1 \pm M} \pm \frac{\Phi^{\pm}_{NI}}{2k_o^2} + \cancelto{\ll 1}{O(\delta^2 M^2)}. \tag{34}$$

The final analytical solution for acoustic pressure (Eq. (25)), requires the integrals to be evaluated. Integration of Terms 1 and 2 in $a^{\pm}$ (Eq. (31)) is straightforward, while for Terms 3 it depends on the duct shape and temperature profile. For Terms 1:

$$\int_{x_1}^{x} \left(-\frac{\alpha}{2} - \frac{\beta}{4}\right) \mathrm{d}x = \frac{-1}{2} \ln\left(\frac{A}{A_1}\sqrt{\frac{T}{T_1}}\right), \tag{35}$$

where A_1, and T_1 represent the duct area and temperature at the inlet ($x = x_1$) respectively. For Terms 2, the Mach number gradient (from Eqs. (12), (15)) is used to evaluate the integral:

$$\frac{1}{M}\frac{\mathrm{d}M}{\mathrm{d}x} = \left(\frac{\beta}{2} - \alpha\right) + (\beta - \alpha)\gamma M^2 + \cancelto{0}{O(M^4)} \Longrightarrow \left(\frac{\beta}{2} - \alpha\right)M = \frac{\mathrm{d}M}{\mathrm{d}x}; \qquad \left(\frac{\beta}{2} - \alpha\right)M^2 = M\frac{\mathrm{d}M}{\mathrm{d}x}. \tag{36}$$

With the final expressions for $a^{\pm}$, $b^{\pm}$, and the definition of acoustic pressure given by Eq. (25), the principle of superposition allows the overall analytical solution for the pressure to be expressed as,

$$\hat{p}(x, \omega) = C_1^+ P_1^+(x, \omega) + C_1^- P_1^-(x, \omega), \tag{37}$$

with constants C_1^+ and C_1^- that are determined using boundary conditions and,

$$P_1^{\pm} = \left(\frac{A_1}{A}\right)^{1/2}\left(\frac{T_1}{T}\right)^{1/4}\left[\frac{\exp\left(\frac{M^2}{2} \mp M + \frac{\gamma}{2}\int_{x_1}^{x}(\alpha M^2 \mp \beta M)\mathrm{d}x^*\right)}{\exp\left(\frac{M_1^2}{2} \mp M_1\right)}\right]\exp\left(\int_{x_1}^{x} \mathrm{i}\left(\frac{\mp k_o}{1 \pm M} \pm \frac{\Phi^{\pm}_{NI}}{2k_o}\right)\mathrm{d}x^*\right), \tag{38}$$

where M_1 is the inlet Mach number. The explicit dependence of the solution on the area and mean temperature profiles is apparent. The amplitude part of the wave-like solution contains terms which cannot be written in terms of the derivative of the Mach number, and hence appear as an integral in $P_1^{\pm}$ (Eq. (38)).

The velocity perturbation, $\hat{u}$, is determined from Eq. (19) and can be written as,

$$\hat{u}(x, \omega) = \frac{1}{\bar{\rho}\bar{c}}\left(B_1^+ C_1^+ P_1^+ - B_1^- C_1^- P_1^-\right), \tag{39}$$

where,

$$B_1^{\pm} = \frac{\mathrm{i}k_o\left(1 - \gamma M^2\right) \pm \frac{\beta}{4} \pm \frac{\alpha}{2} - \alpha M + \frac{\beta M}{2}(1 + \gamma) \pm \frac{\beta M^2}{4}(3\gamma - 7) \pm \frac{\alpha M^2}{2}(3 - 2\gamma)}{\mathrm{i}k_o\left(1 - \gamma M^2\right) + (\beta - 2\alpha)M}. \tag{40}$$

2.2. Frequency range of validity for semi-analytical solution

2.2.1. Lower frequency limit

The analytical solution derived using the WKB method assumes high frequency. We now determine an analytical expression for this high frequency criterion. For a uniform mean-flow, without temperature or area gradients, the upstream and downstream propagating planar wave amplitudes are completely uncoupled and are independent of axial coordinate. The coupling and axial evolution that arises in the presence of axial gradients is mainly caused due to the temperature and area gradients along the flow, with variations in the mean-flow having only a secondary contribution [46].

The high frequency assumption of the WKB method sets the lower frequency limit. This follows from the terms that are neglected in WKB analysis when making the high frequency approximation. It can be interpreted as a "decoupling criterion", as it ensures that the effect of the upstream and downstream propagating plane wave amplitudes on each other is minimal. The terms neglected in the second iteration of $b^{\pm}$ in Eq. (32) ($\Phi^{\pm}_{NI}/k_o^2$ is $\ll 1$) set this limit, thus,

$$f^*_{low} = \frac{\bar{c}_x}{2\pi}\max\sqrt{\left|\frac{\alpha^2}{4} + \frac{3\beta^2}{16} + \frac{\alpha\beta}{2} \mp M\left(\alpha^2 + \frac{\beta^2}{2}(1 - \gamma) - \frac{\alpha\beta}{2}(3 - \gamma)\right) + \frac{\mathrm{d}\alpha}{\mathrm{d}x}\left(\frac{1}{2} \pm M\right) + \frac{1}{2}\frac{\mathrm{d}\beta}{\mathrm{d}x}\left(\frac{1}{2} \pm M(\gamma - 1)\right)\right|}, \tag{41}$$

where the "max" function gives the maximum value of the lower frequency limit evaluated along the duct, $\pm$ corresponds to upstream and downstream propagating plane wave amplitudes, and $\bar{c}_x$ is the local speed of sound.

2.2.2. Upper frequency limit

The analytical solution is valid for planar acoustic waves, which means that higher order acoustic modes such as circumferential and radial modes must be cut-off. This then sets an upper limit on the frequency that can be considered. The frequency at which the first non-planar modes are cut-on in a duct with circular cross-section at a given x is given by,

$$f^*_{high} = \frac{0.293\bar{c}_x}{r_x}, \tag{42}$$

where, r_x is the radius of the duct at x.

To summarise, these expressions for determining the acoustic pressure (Eq. (38)) and acoustic velocity (Eqs. (39) and (40)) are presented for the first time, and are an important result of this work. Beyond the assumptions outlined in the derivation of governing ODE for acoustic pressure, (i) terms of order $O(\delta^2 M^2)$ are further neglected, and (ii) the imaginary part of wave-number (k_o) is assumed very small compared to the real part. The expression for $P_1^{\pm}$ given by Eq. (38) applies for any duct shape/area variation and temperature profile; it requires increased computational effort as the integrals of phase and amplitude need to be determined numerically. A simplified analytical solution can be developed for given area and temperature profiles by evaluating the integrals in Eq. (38). For example, for simple conical and exponentially-shaped ducts with linear temperature variations, a fully analytical solution that depends only on the local mean-flow and thermodynamic properties can be derived at the cost of restricted Mach numbers ($M^2 \ll 1$) and is presented in the Section 2.3.

2.3. Semi-analytical solution for non-isentropic flow in a conical-shaped duct

The accuracy of the proposed semi-analytical solution for the non-isentropic case is evaluated by applying it to two test duct geometries: the conical-shaped duct, shown on the left of Fig. 2 and the exponential-shaped duct shown on the right. The analytical results are compared to the simulation results from the two-linearised Euler equations (Eqs. (5) and (6)) which also neglect the acoustic-entropy coupling.

For the conical-shaped duct, the radius changes linearly with space coordinate, x, with the cross-sectional area then proportional to r_x^2. For a duct of length l, inlet at $x = x_1$, inlet radius r_1, and exit radius r_2, the cross-sectional area varies as,

$$A(x) = A_1(1+\mathcal{A}x)^2, \quad \text{where } \mathcal{A} = \frac{(r_2 - r_1)}{r_1\, l} \text{ and } x \in [x_1, x_1 + l], \tag{43}$$

The area gradient parameter, α, and its spatial derivative become,

$$\alpha = \frac{1}{A}\frac{\mathrm{d}A}{\mathrm{d}x} = \frac{2\mathcal{A}}{(1+\mathcal{A}x)} \Rightarrow \frac{\mathrm{d}\alpha}{\mathrm{d}x} = -\frac{\alpha^2}{2}.$$

Also considering a linear mean-temperature variation ($\overline{T}_1$ at the inlet $(x = x_1)$ and $\overline{T}_2$ at the outlet $(x = x_2)$):

$$\overline{T}(x) = \overline{T}_1(1+\mathcal{B}x), \quad \text{where } \mathcal{B} = \frac{\overline{T}_2 - \overline{T}_1}{\overline{T}_1 l} \text{ and } x \in [x_1, x_1 + l]. \tag{44, 45}$$

Hence,

$$\beta = \frac{\mathcal{B}}{1+\mathcal{B}x} \Rightarrow \frac{\mathrm{d}\beta}{\mathrm{d}x} = \frac{-\mathcal{B}^2}{(1+\mathcal{B}x)^2} = -\beta^2.$$

The analytical solution requires evaluation of the $b^{\pm}$ terms in the integral in order to evaluate the phase. This can be achieved to reasonable accuracy by assuming the flow Mach number to have the following simplified dependence on area and mean-temperature,

$$\frac{M}{M_1} \approx \frac{A_1}{A}\sqrt{\frac{\overline{T}}{\overline{T}_1}}. \tag{47, 48}$$

This simplification is valid for Mach numbers below approximately 0.3 to an (order of $O(M^2)$ accuracy), and hence is justified as the Mach numbers in this analysis are limited in any case by having neglected the acoustic-entropy coupling [46,52]. Using the expressions for $\frac{\mathrm{d}\alpha}{\mathrm{d}x}$ (Eq. (45)) and $\frac{\mathrm{d}\beta}{\mathrm{d}x}$ (Eq. (48)) for $\Phi_{NI}^{\pm}$, $b^{\pm}$ is evaluated as,

$$\int_{x_1}^{x} b^{\pm}\mathrm{d}x = \mp\int_{x_1}^{x}\frac{k_o}{1\pm M}\mathrm{d}x^* \pm \int_{x_1}^{x}\frac{\Phi_{NI}^{\pm}}{2k_o}\mathrm{d}x^* \approx \overbrace{\int_{x_1}^{x}\mp k_o\left(1\mp M + M^2\right)\mathrm{d}x^*}^{\mathbf{I_o^c}} \pm \overbrace{\int_{x_1}^{x}\left(\frac{\alpha\beta}{4k_o} - \frac{\beta^2}{32k_o} \mp \frac{3\alpha^2 M}{4k_o} \pm \frac{\alpha\beta M}{4k_o}(3-\gamma)\right)\mathrm{d}x^*}^{\mathbf{I_1^c}\ to\ I_4^c}. \tag{50}$$

It then follows that,

$$P_1^{\pm} = \left(\frac{A_1}{A}\right)^{1/2}\left(\frac{\overline{T}_1}{\overline{T}}\right)^{1/4}\left[\exp\left(\frac{M^2 - M_1^2}{2} \mp (M - M_1) + J_1^c \mp J_2^c \mp \mathrm{i}I_0^c \pm \mathrm{i}(I_1^c + I_2^c + I_3^c + I_4^c)\right)\right], \tag{51}$$

where J_1^c and J_2^c represent the integral of Terms 3 in $a^{\pm}$ and I_0^c to I_4^c are given as,

$$J_1^c = \int_{x_1}^{x} \frac{\alpha\gamma M^2}{2} \mathrm{d}x^* = \frac{\gamma M_1^2}{12\mathcal{A}}\left[(\mathcal{B}+3\mathcal{A}) - \frac{4\mathcal{A}\mathcal{B}x+\mathcal{B}+3\mathcal{A}}{(1+\mathcal{A}x)^4}\right], \tag{52}$$

$$J_2^c = \mp\int_{x_1}^{x} \frac{\beta\gamma M}{2}\mathrm{d}x^* = \frac{\mathcal{B}M_1}{\mathcal{B}-\mathcal{A}}\left[\frac{\mathcal{B}}{\sqrt{\mathcal{A}(\mathcal{B}-\mathcal{A})}}\left(\tan^{-1}\sqrt{\frac{\mathcal{A}(1+\mathcal{B}x)}{\mathcal{B}-\mathcal{A}}} - \tan^{-1}\sqrt{\frac{\mathcal{A}}{\mathcal{B}-\mathcal{A}}}\right) + \frac{\sqrt{1+\mathcal{B}x}}{1+\mathcal{A}x} - 1\right], \tag{53}$$

$$I_0^c = \int_{x_1}^{x} k_o\left(1 \mp M + M^2\right)\mathrm{d}x^* = k_1\int_{x_1}^{x}\left(\frac{1}{\sqrt{1+\mathcal{B}x}} \mp \frac{M_1}{(1+\mathcal{A}x)^2} + \frac{M_1^2\sqrt{1+\mathcal{B}x)}}{(1+\mathcal{A}x)^4}\right)\mathrm{d}x^*, \tag{54}$$

$$= \frac{2k_1}{\mathcal{B}}\left(\sqrt{1+\mathcal{B}x}-1\right)$$

$$\mp \frac{k_1M_1x}{1+\mathcal{A}x} + k_1M_1^2\left[\frac{\mathcal{B}^3\tan^{-1}\left(\sqrt{\frac{\mathcal{A}(1+\mathcal{B}x)}{\mathcal{B}-\mathcal{A}}}\right)}{8\mathcal{A}^{3/2}(\mathcal{B}-\mathcal{A})^{5/2}} + \frac{\sqrt{1+\mathcal{B}x}\,(\mathcal{B}(\mathcal{A}x+3)-2\mathcal{A})(\mathcal{B}(3\mathcal{A}x-1)+4\mathcal{A})}{24\mathcal{A}(\mathcal{B}-\mathcal{A})^2(1+\mathcal{A}x)^3}\right]_{x_1=0}^{x} \tag{55}$$

$$I_1^c = \frac{1}{2}\int_{x_1}^{x}\frac{\alpha\beta}{2k_o}\mathrm{d}x^* = \frac{\mathcal{A}\mathcal{B}}{k_1\sqrt{\mathcal{A}(\mathcal{B}-\mathcal{A})}}\left[\tan^{-1}\left(\sqrt{\frac{\mathcal{A}(1+\mathcal{B}x)}{\mathcal{B}-\mathcal{A}}}\right) - \tan^{-1}\left(\sqrt{\frac{\mathcal{A}}{\mathcal{B}-\mathcal{A}}}\right)\right], \tag{56}$$

$$I_2^c = \frac{-1}{16}\int_{x_1}^{x}\frac{\beta^2}{2k_o}\mathrm{d}x^* = \frac{\mathcal{B}}{16k_1}\left(\frac{1}{\sqrt{1+\mathcal{B}x}}-1\right), \tag{57}$$

$$I_3^c = \mp\frac{3}{2}\int_{x_1}^{x}\frac{\alpha^2 M}{2k_o}\mathrm{d}x^* = \mp\frac{M_1}{2k_1}\left[(\mathcal{B}+2\mathcal{A}) - \frac{3\mathcal{A}\mathcal{B}x+\mathcal{B}+2\mathcal{A}}{(1+\mathcal{A}x)^3}\right], \tag{58}$$

$$I_4^c = \pm\frac{3-\gamma}{2}\int_{x_1}^{x}\frac{\alpha\beta M}{2k_o}\mathrm{d}x^* = \mp\frac{(3-\gamma)\mathcal{B}M_1}{2k_1}\left[\frac{1}{(1+\mathcal{A}x)^2}-1\right]. \tag{59}$$

where k_1 is the wave-number at the inlet. The acoustic pressure solution for non-isentropic flow in a conical duct is given by Eq. (37) with $P_1^{\pm}$ from Eq. (51). The corresponding velocity perturbation, $\hat{u}$, is determined using Eq. (39), where $B_1^{\pm}$ is given by Eq. (40).

2.3.1. Frequency limits

The lower frequency limit given by Eq. (41) can again be simplified using the expressions for $\frac{\mathrm{d}\alpha}{\mathrm{d}x}$ (Eq. (45)) and $\frac{\mathrm{d}\beta}{\mathrm{d}x}$ (Eq. (48)) to give,

$$f_{low}^* = \frac{\bar{c}_x}{2\pi}\max\left(\sqrt{\left|\pm\frac{3\alpha^2 M}{2} - \frac{\beta^2}{16} + \frac{\alpha\beta}{2} \pm \frac{\alpha\beta M}{2}(3-\gamma)\right|}\right). \tag{60}$$

Both the lower and upper frequency limits are calculated at the duct inlet and outlet and are presented in Fig. 2, where it can be seen that an intermediate range exists where all limits are satisfied.

2.3.2. Validation of analytical solution

In order to validate the above analytical solution, it is compared to numerical simulation of the LEEs under the acoustic forcing and boundary conditions summarised in Fig. 1. The two-linearised Euler equations of Eqs. (5) and (6) are simulated (denoted 2LEEs); like the analytical solution, these neglect acoustic-entropy coupling, meaning the predictions should agree for the frequency and Mach ranges over which the analytical solution is valid. At the duct inlet, x_1, the acoustic impedance, Z_1, is specified by the relation between pressure perturbation, $\hat{p}_1$, and velocity perturbation, $\hat{u}_1$, being $\hat{p}_1 = \bar{\rho}_1\bar{c}_1 Z_1\hat{u}_1$. For the duct outlet, Dowling's method [61] is used in which acoustic waves are considered not to have reached the outlet boundary at x_2. This semi-infinite acoustic problem facilitates validation of the solution across a wide range of frequencies. For a prescribed frequency, the resulting initial value problem is amenable to higher-order schemes; the 4th order Runge-Kutta is employed for our solution.

The variations of the acoustic pressure and velocity along the duct are related to the velocity forcing at the duct inlet using the transfer functions below, consistent with the approach used in Li and Morgans [45];

$$F_p(x,f) = \frac{\hat{p}(x,f)}{\bar{\rho}_1\bar{c}_1\hat{u}_1(f)}; \qquad F_u(x,f) = \frac{\hat{u}(x,f)}{\hat{u}_1(f)}; \tag{61, 62}$$

The difference between the analytical and numerical solution is characterised with "error coefficients", which are relative L^2 norms. If N represents the total number of spatial grid points, the pressure and velocity error coefficients are given by,

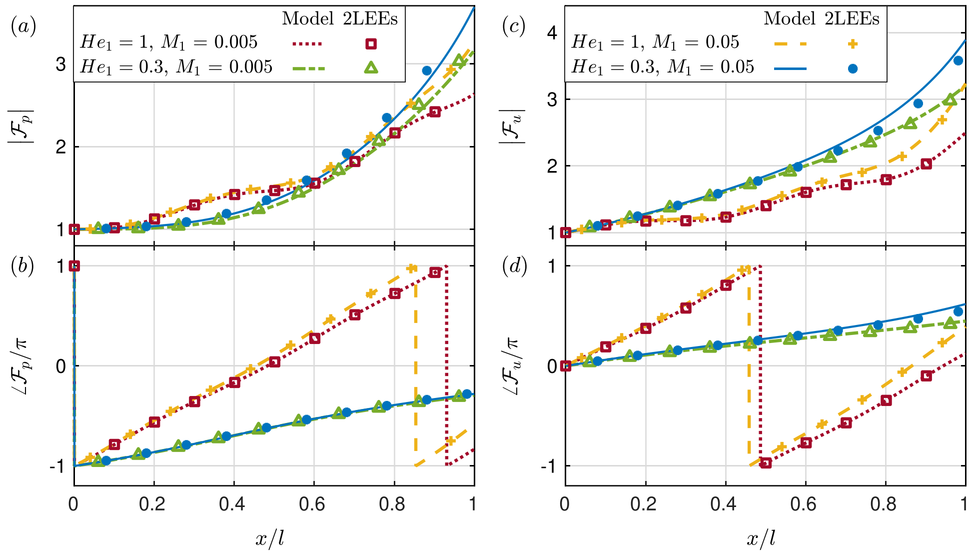

Fig. 3. Evolution of F_p and F_u with x. $\overline{T}_1 = 1600$ K, $\overline{T}_2 = 1200$ K, $M_1 = 0.005$ & 0.05, $M_2 = 0.027$ & 0.27, $He_1 = 1$ & 0.3, and $Z_1 = -1$. (a): transfer function gain $|F_p|$. (b): transfer function phase $\angle F_p$. (c): transfer function gain $|F_u|$. (d): transfer function phase $\angle F_u$.

$$\epsilon_p\left(F_{p,\ Analytical}, F_{p,\ 2LEEs}\right) = \left(\sum_{j=1}^{N}\left|F_{p,\ Analytical}\left(x_j\right) - F_{p,\ 2LEEs}\left(x_j\right)\right|^2 / \sum_{j=1}^{N}\left|F_{p,\ Analytical}\left(x_j\right)\right|^2\right)^{1/2} \tag{63}$$

$$\epsilon_u\left(F_{u,\ Analytical}, F_{u,\ 2LEEs}\right) = \left(\sum_{j=1}^{N}\left|F_{u,\ Analytical}\left(x_j\right) - F_{u,\ 2LEEs}\left(x_j\right)\right|^2 / \sum_{j=1}^{N}\left|F_{u,\ Analytical}\left(x_j\right)\right|^2\right)^{1/2} \tag{64}$$

2.3.3. Validation results

The conical duct in Fig. 2 (left) is initially considered across three different inlet Mach numbers and three different frequencies. The first two frequencies considered satisfy both the lower (Eq. (60)) and upper (Eq. (42)) frequency limits, while the third falls below the lower frequency limit. Note that frequencies are presented as a non-dimensional Helmholtz number based on length of the duct, defined as, $He_1 = fl/\bar{c}_1$.

- **Very low Mach numbers:** Fig. 3 compares the analytical model and numerical 2LEEs solutions when the duct Mach number is $M_1 = 0.005$ at inlet, corresponding to $M_2 = 0.027$ at the duct outlet in the presence of a strong temperature gradient 800 K/m. From Section 2.3.1, at very low Mach numbers, the lower frequency limit of Eq. (60) becomes proportional to β which is generally small in practical engines, meaning that the analytical solution should perform accurately for all frequencies below the cut-on for higher order modes. It is noted that the analytical and numerical solutions are in close agreement, for the frequencies considered.
- **Increased low Mach numbers:** For an inlet duct Mach number of 0.05 and outlet Mach number of 0.27, Fig. 3 shows that the analytical and numerical results agree close to the inlet, but slightly diverge towards the exit for the lower frequency of $He_1 = 0.3$. This is attributed to the increased Mach numbers and α values at the outlet.
- **Frequency below lower frequency limit:** Fig. 4 (plotted in red) compares the predictions for a frequency of 160Hz ($He_1 = 0.1$), which falls below the lower frequency limit of Eq. (60). It is observed that even for the very low Mach numbers, while the acoustic pressure is well-captured, a deviation in the phase of F_u occurs.
- **High subsonic Mach numbers:** Fig. 4 also compares predictions for a duct with outlet Mach number 0.73. Due to the low Mach assumption used in deriving Eq. (51), $P_1^{\pm}$ is predicted using the general solution (Eq. (38)) at these high subsonic Mach numbers. Although this general solution requires slightly increased computational effort to evaluate the integrals, the prediction is accurate. The solution now depends on upstream mean-flow and thermodynamic properties.
- **Effect of flow temperature:** The errors in the acoustic pressure and velocity predictions (Eqs. (63) and (64)) are shown in Fig. 5 as a function of mean-temperature variation and non-dimensional frequency. The corresponding values of flow Mach number at the outlet, M_2, are shown on a separate axis. The error remains below $<$ 10% over most conditions.
- **Effect of flow Mach number - using simplified low Mach solution:** The effect of flow Mach number on the acoustic pressure and velocity errors is shown in Fig. 6 for a range of inlet Helmholtz numbers. The acoustic field is predicted

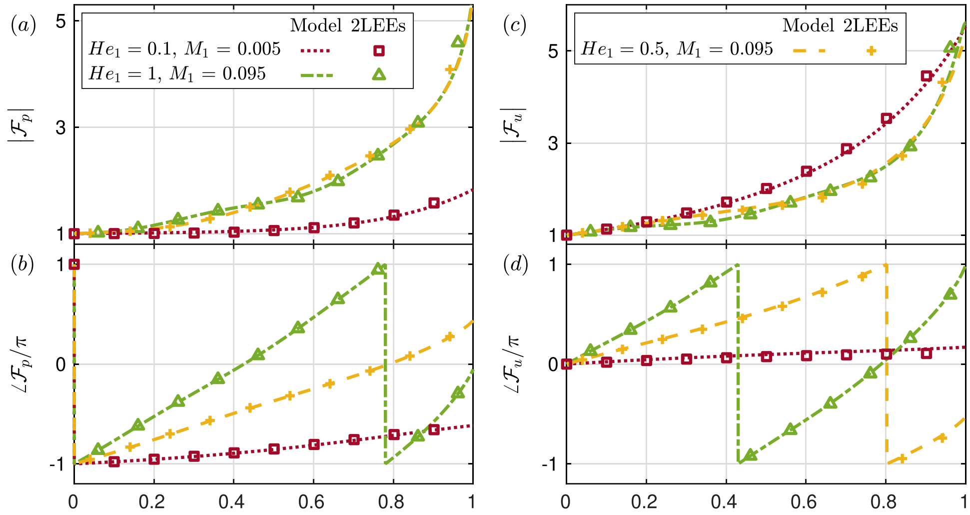

Fig. 4. Evolution of F_p and F_u with x. $\overline{T}_1 = 1600$ K, $\overline{T}_2 = 1200$ K, $M_1 = 0.005$ & 0.095, $M_2 = 0.05$ & 0.73, Helmholtz numbers given by He_1, and $Z_1 = -1$. (a): transfer function gain $|F_p|$. (b): transfer function phase $\angle F_p$. (c): transfer function gain $|F_u|$. (d): transfer function phase $\angle F_u$.

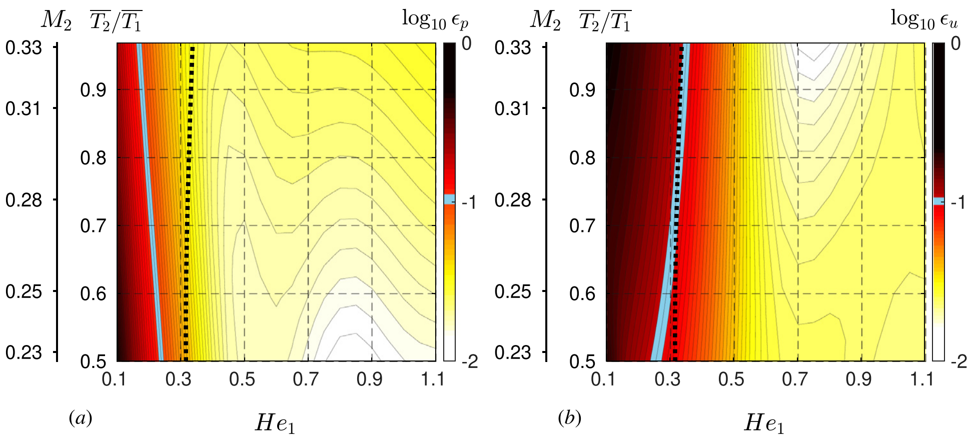

Fig. 5. Contour maps of (a) ϵ_p and (b) ϵ_u using the proposed analytical model as functions of He_1 and $\overline{T}_2/\overline{T}_1$, in conical test-case. The dashed line represents the lower frequency limit given by Eq. (60).

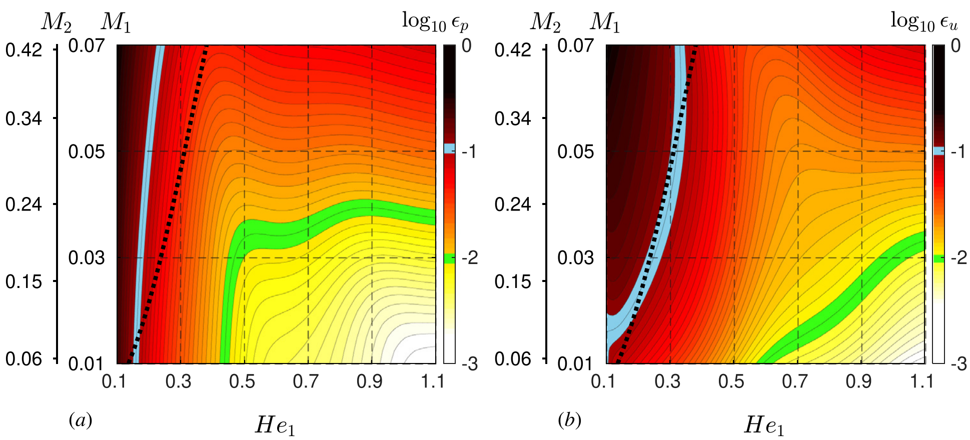

Fig. 6. Contour maps of (a) ϵ_p and (b) ϵ_u using the proposed analytical model as functions of He_1 and M_1, in conical test-case. The dashed line represents the lower frequency limit given by Eq. (60).

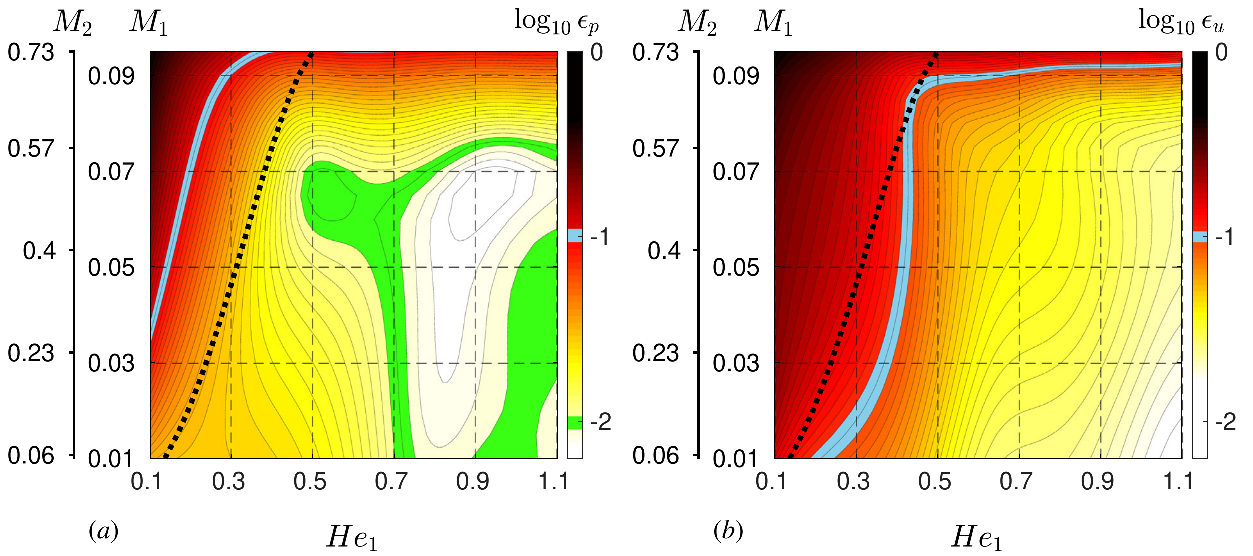

Fig. 7. Contour maps of (a) ϵ_p and (b) ϵ_u using the general analytical solution as functions of He_1 and M_1, in conical test-case. The dashed line represents the lower frequency limit given by Eq. (41).

using the simplified solution (Eq. (51)), which is valid for small Mach numbers. The error remains below 10% over most conditions, except when both the Mach number is high and the frequency is low.

- **Effect of flow Mach number - using general solution** : As discussed earlier, for ducts sustaining high subsonic flow Mach numbers, $P_1^{\pm}$ can be estimated using the general solution given by Eq. (38), at marginally increased computational effort. The errors in acoustic pressure and velocity shown in Fig. 7 illustrate that this solution can be employed over an increased range of flow Mach numbers and frequencies, while keeping the error below 10%.

2.4. Semi-analytical solution for non-isentropic flow in an exponentially-shaped duct

We now consider the semi-analytical solution for a duct whose area convergence is exponential in shape with a linearly varying mean-temperature, as shown on the right of Fig. 2. If at the duct inlet $(x = x_1)$ area is A_1 then:

$$A(x) = A_1 e^{\alpha x}, \quad \text{where } \alpha = \frac{1}{A}\frac{\mathrm{d}A}{\mathrm{d}x} = \text{Constant} \quad \Rightarrow \frac{\mathrm{d}\alpha}{\mathrm{d}x} = 0 \text{ and } x \in [x_1, x_1 + l]. \tag{65, 66}$$

Using the expressions for area variation (Eqs. (65), (66)) and temperature variation (Eqs. (47), (48)), the integrals given in $P_1^{\pm}$ (Eq. (38)) are evaluated in a similar manner as for the conical-shaped duct.

$$P_1^{\pm} = \left(\frac{A_1}{A}\right)^{1/2}\left(\frac{\overline{T}_1}{\overline{T}}\right)^{1/4}\left[\exp\left(\frac{M^2 - M_1^2}{2} \mp (M - M_1) + J_1^e \mp J_2^e \mp \mathrm{i}I_0^e \pm \mathrm{i}(I_1^e + I_2^e + I_3^e + I_4^e + I_5^e)\right)\right]. \tag{67}$$

The various terms are given by the following:

$$J_1^e = \int_{x_1}^{x} \frac{\alpha\gamma M^2}{2}\mathrm{d}x^* = \frac{\gamma M_1^2}{8\alpha}[(\mathcal{B} + 2\alpha) - (\mathcal{B} + 2\alpha + 2\alpha\mathcal{B}x)\exp(-2\alpha x)], \tag{68}$$

$$J_2^e = \mp\int_{x_1}^{x} \frac{\beta\gamma M}{2}\mathrm{d}x^* = \mp\sqrt{\frac{\pi\mathcal{B}}{\alpha}}\frac{\gamma M_1}{2}\exp\left(\frac{\alpha}{\mathcal{B}}\right)\left[\mathrm{erf}\left(\sqrt{\frac{\alpha(1 + \mathcal{B}x)}{\mathcal{B}}}\right) - \mathrm{erf}\left(\sqrt{\frac{\alpha}{\mathcal{B}}}\right)\right], \tag{69}$$

$$\begin{aligned} I_0^e = \int_{x_1}^{x} k_o\left(1 \mp M + M^2\right)\mathrm{d}x^* &= \frac{2k_1}{\mathcal{B}}\left(\sqrt{1 + \mathcal{B}x} - 1\right) \pm \frac{M_1 k_1}{\alpha}(\exp(-\alpha x) - 1) \\ &+ \frac{k_1 M_1^2}{2\alpha}\left[\frac{1}{2}\sqrt{\frac{\pi\mathcal{B}}{2\alpha}}\exp\left(\frac{2\alpha}{\mathcal{B}}\right)\left(\mathrm{erf}\left(\sqrt{\frac{2\alpha}{\mathcal{B}}(1 + \mathcal{B}x)}\right) - \mathrm{erf}\left(\sqrt{\frac{2\alpha}{\mathcal{B}}}\right)\right) - \sqrt{1 + \mathcal{B}x}\exp(-2\alpha x) + 1\right], \end{aligned} \tag{70}$$

$$I_1^e = \frac{1}{4}\int_{x_1}^{x} \frac{\alpha^2}{2k_o}\mathrm{d}x^* = \frac{\alpha^2}{12\mathcal{B}k_1}\left((1 + \mathcal{B}x)^{3/2} - 1\right), \tag{71}$$

$$I_2^e = -\frac{1}{16}\int_{x_1}^{x} \frac{\beta^2}{2k_o}\mathrm{d}x^* = \frac{\mathcal{B}}{16k_1}\left[\frac{1}{\sqrt{1 + \mathcal{B}x}} - 1\right], \tag{72}$$

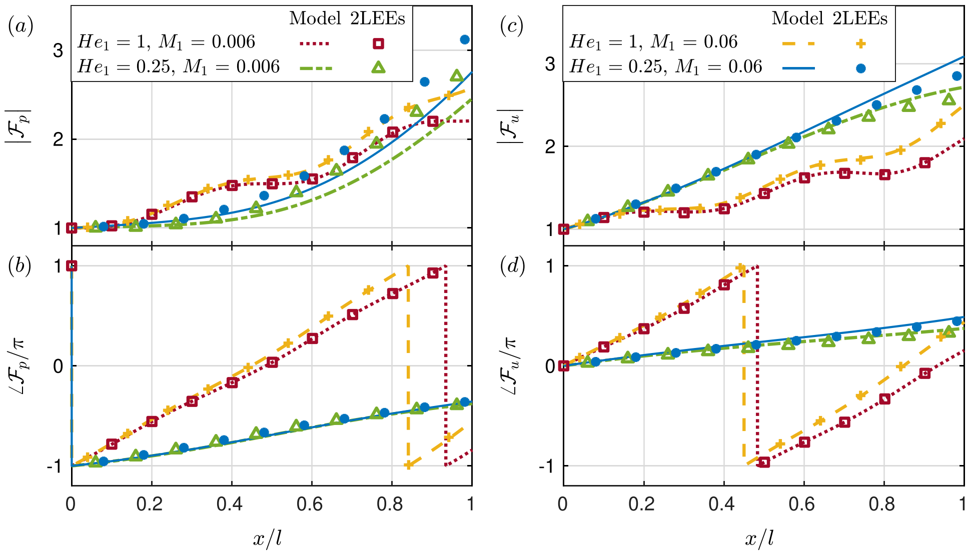

Fig. 8. Evolution of F_p and F_u with x. $\overline{T}_1 = 1600$ K, $\overline{T}_2 = 1200$ K, $M_1 = 0.006$ & 0.06, $M_2 = 0.027$ & 0.28, $He_1 = 1$ & 0.25, and $Z_1 = -1$. (a): transfer function gain $|F_p|$. (b): transfer function phase $\angle F_p$. (c): transfer function gain $|F_u|$. (d): transfer function phase $\angle F_u$.

$$I_3^e = \frac{1}{2}\int_{x_1}^{x}\frac{\alpha\beta}{2k_o}\mathrm{d}x^* = \frac{\alpha}{2k_1}\left[\sqrt{1+\mathcal{B}x}-1\right], \tag{73}$$

$$I_4^e = \mp\int_{x_1}^{x}\frac{\alpha^2 M}{2k_o}\mathrm{d}x^* = \pm\frac{M_1}{2k_1}[(\alpha+\mathcal{B}+\alpha\mathcal{B}x)\exp(-\alpha x)-(\alpha+\mathcal{B})], \tag{74}$$

$$I_5^e = \pm\frac{(3-\gamma)}{2}\int_{x_1}^{x}\frac{\alpha\beta M}{2k_o}\mathrm{d}x^* = \pm\frac{(3-\gamma)\mathcal{B}M_1}{4k_1}[1-\exp(-\alpha x)]. \tag{75}$$

The velocity perturbation, $\hat{u}$, is given by Eq. (39), where $B_1^{\pm}$ is from Eq. (40) and $P_1^{\pm}$ from Eq. (67).

2.4.1. Frequency limits

The lower frequency limit is obtained by simplifying Eq. (41) using $\frac{\mathrm{d}\alpha}{\mathrm{d}x}$ (Eq. (66)) and $\frac{\mathrm{d}\beta}{\mathrm{d}x}$ (Eq. (48)) to give,

$$f_{low}^* = \frac{\bar{c}_x}{2\pi}\ \max\sqrt{\left|\frac{\alpha^2}{4}-\frac{\beta^2}{16}+\frac{\alpha\beta}{2}\mp M\left(\alpha^2-\frac{\alpha\beta}{2}(3-\gamma)\right)\right|}. \tag{76}$$

It shows stronger dependence on α than the conical-shaped duct, with the very low Mach limit being $|k_o| \gg |\alpha|$ and $|k_o| \gg |\beta|$, implying the possibility for errors at even very low Mach numbers and frequencies. The lower and upper frequency limits as calculated at both the duct inlet and outlet are shown in the right of Fig. 2. At the duct inlet, the lower frequency limit is higher than for the conical-shaped duct.

- **Very low Mach numbers:** For a Mach number of $M_1 = 0.006$ at the inlet and $M_2 = 0.027$ at the outlet, Fig. 8 compares the analytical model solution with numerical 2LEEs solution. The results agree well at high frequencies but diverge for lower frequencies. This is attributed to the dependence in the frequency limit of Eq. (76) on the dominant α term.
- **Increased low Mach numbers:** For a Mach number of 0.06 at the inlet and 0.28 at the outlet, the results in Fig. 8 are only subtly different to those at very low Mach numbers. A slight deviation is observed throughout the length, confirming the strong dependence on α for exponential-shaped ducts.

- **Effect of flow Mach number:** The errors in the acoustic pressure and velocity predictions (Eqs. (63) and (64)) are shown in Fig. 9 as a function of both flow Mach number and non-dimensionalised frequency. Above an inlet Helmholtz number of 0.3, the error remains below 10%.
- **Effect of changing duct convergence:** For a flow Mach number of 0.035 at the inlet, the rate of area change of the exponential duct is varied through the α term. The errors in the acoustic pressure and velocity are shown in Fig. 10; the error remains below 10% unless both the area gradient is steep and the frequency low.

To summarise, the planar wave amplitudes for conical and exponential-shaped ducts are given by Eqs. (51) and (67) respectively, for the case of a non-isentropic 1-D mean flow. The wave amplitudes vary with position along the duct, x, and

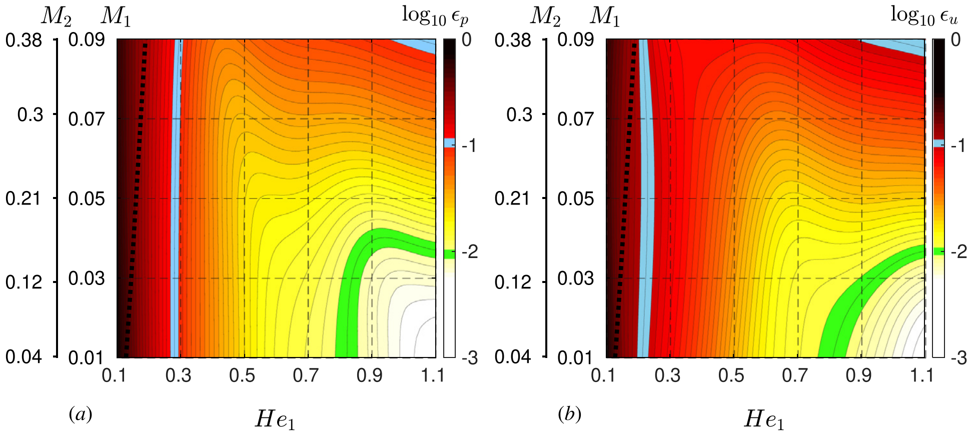

Fig. 9. Contour maps of (a) ϵ_p and (b) ϵ_u using the proposed analytical model as functions of He_1 and M_1, in exponential test-case. The dashed line represents the lower frequency limit given by Eq. (76).

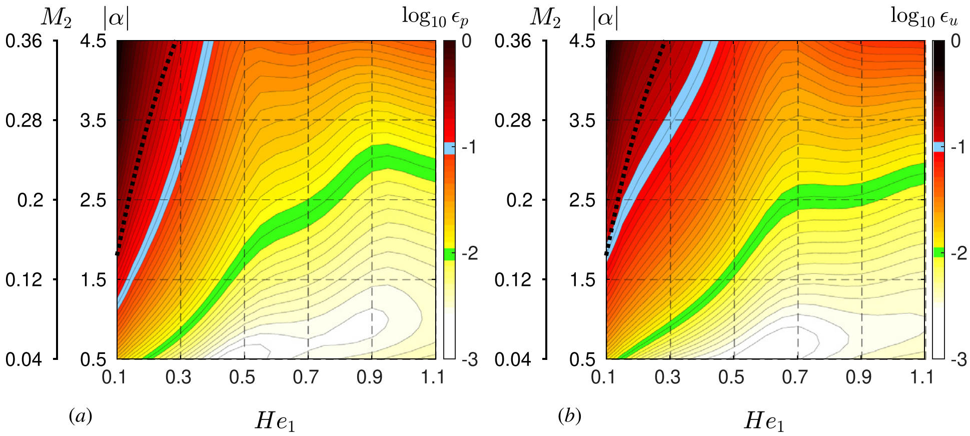

Fig. 10. Contour maps of (a) ϵ_p and (b) ϵ_u using the proposed analytical model as functions of He_1 and α, in exponential test-case. The dashed line represents the lower frequency limit given by Eq. (76).

are only functions of inlet condition, Mach number, area and temperature variation parameters; they are straightforward to compute. Further to the assumptions outlined for deriving the general solution, it is also assumed that $M^2 \ll 1$, to facilitate using simplified Mach expressions for evaluating the integrals.

3. Isentropic varying area flows

A flow in which the effects of fluid viscosity, thermal conductivity, and heat sources are negligible can be described as isentropic. As the net heat-flux from the system, $\bar{\dot{Q}}$ (Eq. (11)), is zero for an isentropic flow, the gradients of area and mean-temperature are related:

$$\bar{\dot{Q}} = 0 \quad \Rightarrow \quad \beta = \frac{\alpha M^2(\gamma-1)}{1-M^2}. \tag{77}$$

The linearized isentropic flow conservation equations for mass, momentum, and energy presented by Marble and Candel [36], are converted to frequency domain (again by assuming a time-dependence of the form $y' = \hat{y}e^{i\omega t}$) as follows,

$$\left(i\omega + \gamma M^2\frac{d\bar{u}}{dx}\right)\hat{p} + \bar{u}\frac{d\hat{p}}{dx} + \frac{1}{M^2}\frac{d\bar{p}}{dx}\hat{u} + \gamma\bar{p}\frac{d\hat{u}}{dx} = 0, \tag{78}$$

$$\left(i\omega + \frac{d\bar{u}}{dx}\right)\hat{u} + \bar{u}\frac{d\hat{u}}{dx} + \bar{u}\frac{d\bar{u}}{dx}\frac{\hat{p}}{\gamma\bar{p}} + \frac{1}{\bar{\rho}}\frac{d\hat{p}}{dx} = \cancelto{\sim 0}{\bar{u}\frac{d\bar{u}}{dx}\hat{\sigma}}, \tag{79}$$

$$i\omega\hat{\sigma} + \bar{u}\frac{d\hat{\sigma}}{dx} = 0. \tag{80}$$

The above set of equations can also be obtained by substituting for β (using Eq. (77)) in the linearized Euler equations for non-isentropic flow (Eqs. (5)–(7)). The source-term of the linearized energy equation (Eq. (80)) is zero, this implies that an entropy disturbance at the inlet simply advects through the duct, its magnitude unchanged. Using the relation between the area and mean-temperature variations (Eq. (77)), a governing homogenous ODE in terms of $\hat{p}$ is obtained from Eq. (21):

$$\left(1 - M^2 + \frac{2\alpha M}{\mathrm{i}k_o} - \frac{4\alpha^2 M^2}{k_o^2}\right)\frac{\mathrm{d}^2\hat{p}}{\mathrm{d}x^2} - \left(2\mathrm{i}Mk_o - \alpha + 2\alpha M^2 - \frac{2M}{\mathrm{i}k_o}\frac{\mathrm{d}\alpha}{\mathrm{d}x}\right)\frac{\mathrm{d}\hat{p}}{\mathrm{d}x} + \left({k_o}^2 + 3\alpha^2 M^2 - 3M^2\frac{\mathrm{d}\alpha}{\mathrm{d}x}\right)\hat{p} = 0. \quad (81)$$

The iterative WKB based method is again used to determine the analytical solution for acoustic pressure in terms of upstream and downstream propagating wave amplitudes using Eq. (37) where,

$$P_1^{\pm} = \left(\frac{A_1}{A}\right)^{1/2}\left[\frac{\exp\left(M_1^2\left(\frac{\gamma-3}{8}\right) \pm M_1 \mp M_1^3\left(\frac{\gamma-1}{3}\right)\right)}{\exp\left(M^2\left(\frac{\gamma-3}{8}\right) \pm M \mp M^3\left(\frac{\gamma-1}{3}\right)\right)}\right]\exp\left(\int_{x_1}^{x}\mathrm{i}\left(\frac{\mp k_o}{1 \pm M} \pm \frac{\Phi_I^{\pm}}{2k_o}\right)\mathrm{d}x^*\right), \quad (82)$$

with,

$$\frac{\Phi_I^{\pm}}{k_o^2} = \frac{\delta^2}{4} \mp \delta^2 M + \kappa\delta^2\left(\frac{1}{2} \pm M\right) + \mathrm{O}(\delta^2 M^2), \quad \text{where } \delta = \frac{\alpha}{k_o}, \quad (83)$$

and M_1, A_1 again represent the Mach-number of the flow and cross-sectional area of the duct respectively at $x = x_1$.

The corresponding velocity perturbation, $\hat{u}$, is determined using Eq. (39), where $B_1^{\pm}$ is given by Eq. (84).

$$B_1^{\pm} = \frac{1}{\mathrm{i}k_o\left(1 - M^2\right) - 2\alpha M}\left[\mathrm{i}k_o\left(1 - M^2\right) \pm \frac{\alpha}{2} - \alpha M \mp \frac{\alpha M^2(\gamma - 3)}{4} + \frac{\alpha M^3(\gamma + 1)}{2}\right]. \quad (84)$$

3.1. Analytical solution for isentropic flow in a conical-shaped duct

Similar to the non-isentropic flow case, the solution can be further simplified assuming the Mach-number to vary as $M = M_1 A_1/A$. Furthermore, the temperature variation, β, and thereby wave-number, k_o, variation, is assumed low enough to be taken as constant in the integration. This is a good approximation for isentropic flows: for example, for the geometry of Fig. 2(left), for an isentropic mean flow the wave-number (k_o) only changes by 2% over the domain. This simplification leads to,

$$P_1^{+} = \left(\frac{A_1}{A}\right)^{1/2}\left[\frac{\exp\left(M_1^2\left(\frac{\gamma-3}{8}\right) + M_1 - M_1^3\left(\frac{\gamma-1}{3}\right) - \mathrm{i}k_o\left[x - \frac{\sqrt{M_1}}{\mathcal{A}}\tan^{-1}\left(\frac{\mathcal{A}x\sqrt{M_1}}{1+\mathcal{A}x+M_1}\right) + \frac{\mathcal{A}M_1}{k_o^2}\left(1 - \frac{1}{(1+\mathcal{A}x)^3}\right)\right]\right)}{\exp\left(M^2\left(\frac{\gamma-3}{8}\right) + M - M^3\left(\frac{\gamma-1}{3}\right)\right)}\right], \quad (85a)$$

$$P_1^{-} = \left(\frac{A_1}{A}\right)^{1/2}\left[\frac{\exp\left(M_1^2\left(\frac{\gamma-3}{8}\right) - M_1 + M_1^3\left(\frac{\gamma-1}{3}\right) + \mathrm{i}k_o\left[x - \frac{\sqrt{M_1}}{2\mathcal{A}}\ln\left(\left(\frac{1-\sqrt{M_1}}{1+\sqrt{M_1}}\right)\left(\frac{1+\sqrt{M_1}+\mathcal{A}x}{1-\sqrt{M_1}+\mathcal{A}x}\right)\right) - \frac{\mathcal{A}M_1}{k_o^2}\left(1 - \frac{1}{(1+\mathcal{A}x)^3}\right)\right]\right)}{\exp\left(M^2\left(\frac{\gamma-3}{8}\right) - M + M^3\left(\frac{\gamma-1}{3}\right)\right)}\right]. \quad (85b)$$

3.2. Semi-analytical solution for isentropic flow in an exponential-shaped duct

The semi-analytical solution when applied to exponential-shaped duct leads to,

$$P_1^{\pm} = \left(\frac{A_1}{A}\right)^{1/2}\left[\frac{\exp\left(M_1^2\left(\frac{\gamma-3}{8}\right) \pm M_1 \mp M_1^3\left(\frac{\gamma-1}{3}\right) \mp \frac{\mathrm{i}k_o}{\alpha}\ln\left(\frac{\exp(\alpha x) \pm M_1}{1 \pm M_1}\right) \pm \frac{\mathrm{i}\alpha^2 x}{8k_o} + \frac{\mathrm{i}\alpha M_1}{2k_o}\left(\exp(-\alpha x) - 1\right)\right)}{\exp\left(M^2\left(\frac{\gamma-3}{8}\right) \pm M \mp M^3\left(\frac{\gamma-1}{3}\right)\right)}\right]. \quad (86)$$

Using $P_1^{\pm}$ from Eq. (85) or Eq. (86), Eq. (37) gives the acoustic pressure solution for isentropic flow in a conical duct or exponential duct respectively. The velocity perturbation, $\hat{u}$, is determined using Eq. (39), where $B_1^{\pm}$ is now given by Eq. (84).

4. Effect of acoustic-entropy coupling on the accuracy of the analytical model

As outlined in Section 1, the analytical solutions in this work are all based upon the assumption that the acoustic-entropy coupling is negligible. This has previously been shown to be the case when Mach numbers are low enough [46,52]. To investigate the degree to which this assumption holds for the geometries and flows considered in this work, the analytical model solutions are now compared to the numerical solution of the three linearised Euler equations, which fully account for acoustic-entropy coupling. A 1% normalised entropy or reduced temperature fluctuation ($\hat{\sigma} \sim T'/\overline{T} = 0.01$) [54], is applied at the inlet and its effect on the acoustic field is studied for a range of Mach numbers and frequencies for the conical-shaped duct. (It has been checked that the acoustic-entropy coupling behaves in a qualitatively similar way for the exponential-shaped duct.)

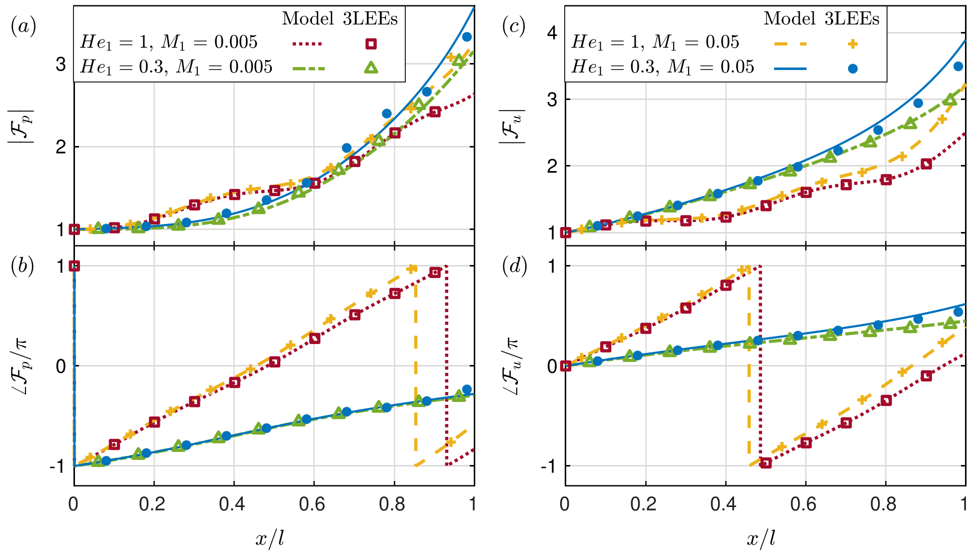

Fig. 11. Evolution of F_p and F_u with x. $\overline{T}_1 = 1600$ K, $\overline{T}_2 = 1200$ K, $\hat{\sigma} = 0.01$, $M_1 = 0.005$ & 0.05, $M_2 = 0.027$ & 0.27, $He_1 = 1$ & 0.3, and $Z_1 = -1$. (a): transfer function gain $|F_p|$. (b): transfer function phase $\angle F_p$. (c): transfer function gain $|F_u|$. (d): transfer function phase $\angle F_u$.

4.1. Non-isentropic flow through conical-shaped duct

- **Very low Mach numbers:** Fig. 11, compares the analytical model and numerical 3LEEs solution for a Mach number of 0.005 at inlet and 0.027 at duct outlet for two different Helmholtz numbers. The analytical solution agrees very well with the numerical one, confirming that the acoustic-entropy coupling is weak at these low Mach numbers.
- **Increased low Mach numbers:** For a Mach number of 0.05 at inlet and 0.27 at outlet, the analytical model and numerical 3LEEs solutions, also presented in Fig. 11, show that in the parts of the duct with higher Mach numbers, small errors in the predicted solution are observable at both Helmholtz numbers.

5. Conclusions

This paper presents an analytical solution for the planar acoustic field in ducts which sustain a 1-D mean flow, vary in cross-sectional area and may exhibit an axial temperature variation. The duct mean flow may be non-isentropic, such that the area and temperature variations can be prescribed independently. A second order homogeneous ordinary differential equation is derived from the linearized conservation equations, by neglecting acoustic-entropy coupling, high Mach number terms and by assuming that the normalised area or temperature gradient occurs slowly in some sense, in that it is much smaller than the wave-number of the acoustics. The second order ODE is solved using an iterative WKB method, which assumes a wave-like solution with separate amplitude and phase factors. The final solution thus obtained is a superposition of upstream and downstream propagating planar waves, whose amplitudes vary axially. These planar wave amplitudes are computationally easy to evaluate and at any location they depend on wave-number, upstream thermodynamic and mean-flow properties, and can be applied for ducts with any arbitrarily varying area and temperature profiles. Further simplified solutions were obtained for specific duct geometries which were conical and exponential in shape with linear temperature gradient; these analytical solutions were validated by comparing to numerical solutions of the linearized flow conservations. The frequency range of validity of the solutions was considered in some detail; the frequency must be low enough for the plane wave assumption to hold, yet high enough for the ODE derivation and WKB assumptions to hold. General analytical limits were derived and the specific frequency values calculated for all of the nozzle flows considered. Within (and even slightly beyond) the calculated frequency ranges of validity, the analytical solutions performed very well. Results are also presented for flows which are isentropic, and which therefore have axial variations of cross-sectional area and temperature are directly related are discussed. Finally, the effect of acoustic-entropy coupling on the accuracy of analytical solution was investigated for the specific nozzle geometries considered in this work, by comparing the solution to the full set of three linearized Euler equations which fully account for acoustic-entropy coupling. The coupling effect was seen to be negigible for sufficiently small duct Mach numbers, consistent with previous findings.

Declaration of Competing Interest

The authors declare that they have no known competing financial interests or personal relationships that could have appeared to influence the work reported in this paper.

CRediT authorship contribution statement

Saikumar R. Yeddula: Conceptualization, Methodology, Software, Validation, Formal analysis, Investigation, Writing - original draft. **Aimee S. Morgans:** Supervision, Writing - review & editing, Project administration, Funding acquisition.

Acknowledgements

The authors would like to acknowledge the European Research Council (ERC) Consolidator Grant AFIRMATIVE (2018–2023) as well as the Inlaks Shivdasani foundation for supporting the research.

References

[1] B.T. Chu, On the energy transfer to small disturbances in fluid flow (Part I), Acta Mech. 1 (3) (1965) 215–234.
[2] M.A. Heckl, Active control of the noise from a rijke tube, in: Aero-and Hydro-acoustics, Springer, Berlin, Heidelberg, 1986, pp. 211–216.
[3] S.M. Candel, Combustion instabilities coupled by pressure waves and their active control, in: Symposium (International) on Combustion, 24, Elsevier, 1992, pp. 1277–1296.
[4] A.P. Dowling, The calculation of thermoacoustic oscillations, J. Sound Vib. 180 (4) (1995) 557–581.
[5] J.J. Keller, W. Egli, J. Hellat, Thermally induced low-frequency oscillations, J. Apll. Math. Phys. 36 (2) (1985) 250–274.
[6] J.J. Keller, Thermoacoustic oscillations in combustion chambers of gas turbines, AIAA J. 33 (12) (1995) 2280–2287.
[7] S. Candel, Combustion dynamics and control: progress and challenges, Proc. Combust. Inst. 29 (1) (2002) 1–28.
[8] A.P. Dowling, S.R. Stow, Acoustic analysis of gas turbine combustors, J. Propul. Power 19 (5) (2003) 751–764.
[9] X. Han, J. Li, A.S. Morgans, Prediction of combustion instability limit cycle oscillations by combining flame describing function simulations with a thermoacoustic network model, Combust. Flame 162 (10) (2015) 3632–3647.
[10] D. Laera, T. Schuller, K. Prieur, D. Durox, S.M. Camporeale, S. Candel, Flame describing function analysis of spinning and standing modes in an annular combustor and comparison with experiments, Combust. Flame 184 (2017) 136–152.
[11] Y. Xia, D. Laera, W.P. Jones, A.S. Morgans, Numerical prediction of the flame describing function and thermoacoustic limit cycle for a pressurised gas turbine combustor, Combust. Sci. Technol. 191 (5–6) (2019) 979–1002.
[12] A. Giauque, L. Selle, L. Gicquel, T. Poinsot, H. Buechner, P. Kaufmann, W. Krebs, System identification of a large-scale swirled partially premixed combustor using LES and measurements, J. Turbul. 1 (6) (2005) N21.
[13] H.J. Krediet, C.H. Beck, W. Krebs, S. Schimek, C.O. Paschereit, J.B. Kok, Identification of the flame describing function of a premixed swirl flame from LES, Combust. Sci. Technol. 184 (7–8) (2012) 888–900.
[14] P. Wolf, G. Staffelbach, L.Y. Gicquel, J.D. Müller, T. Poinsot, Acoustic and large eddy simulation studies of azimuthal modes in annular combustion chambers, Combust. Flame 159 (11) (2012) 3398–3413.
[15] L. Tay-Wo-Chong, W. Polifke, Large eddy simulation-based study of the influence of thermal boundary condition and combustor confinement on premix flame transfer functions, J. Eng. Gas Turbine Power 135 (2) (2013) 021502, doi:10.1115/1.4007734.
[16] S. Wysocki, G. Di-Chiaro, F. Biagioli, Effect of fuel mixture fraction and velocity perturbations on the flame transfer function of swirl stabilized flames, Combust. Theor. Model. 19 (6) (2015) 714–743.
[17] S. Hermeth, G. Staffelbach, L.Y. Gicquel, T. Poinsot, LES evaluation of the effects of equivalence ratio fluctuations on the dynamic flame response in a real gas turbine combustion chamber, Proc. Combust. Inst. 34 (2) (2013) 3165–3173.
[18] X. Han, A.S. Morgans, Simulation of the flame describing function of a turbulent premixed flame using an open-source LES solver, Combust. Flame 162 (5) (2015) 1778–1792.
[19] S. Ruan, T.D. Dunstan, N. Swaminathan, R. Balachandran, Computation of forced premixed flames dynamics, Combust. Sci. Technol. 188 (7) (2016) 1115–1135.
[20] C.Y. Lee, S. Cant, LES of nonlinear saturation in forced turbulent premixed flames, Flow Turbul. Combust. 99 (2) (2017) 461–486.
[21] S. Evesque, W. Polifke, Low-order acoustic modelling for annular combustors: validation and inclusion of modal coupling, in: ASME Turbo Expo 2002: Power for Land, Sea, and Air, volume 1, American Society of Mechanical Engineers Digital Collection, 2002, pp. 321–331.
[22] S. Evesque, W. Polifke, C. Pankiewitz, Spinning and azimuthally standing acoustic modes in annular combustors, in: 9th AIAA/CEAS Aeroacoustics Conference and Exhibit, 2003, p. 3182.
[23] S.R. Stow, A.P. Dowling, A time-domain network model for nonlinear thermoacoustic oscillations, J. Eng. Gas Turbine Power 131 (3) (2009) 031502.
[24] J. Li, A.S. Morgans, Time domain simulations of nonlinear thermoacoustic behaviour in a simple combustor using a wave-based approach, J. Sound Vib. 346 (2015) 345–360.
[25] M. Bauerheim, F. Nicoud, T. Poinsot, Progress in analytical methods to predict and control azimuthal combustion instability modes in annular chambers, Phys. Fluids 28 (2) (2016) 021303.
[26] F. Schaefer, W. Polifke, Low-order network model of a duct with non-uniform cross-section and varying mean temperature in the presence of mean flow, InAIAA Propul. Energy 2019 (2019) 4376.
[27] D. Yang, D. Laera, A.S. Morgans, A systematic study of nonlinear coupling of thermoacoustic modes in annular combustors, Journal of Sound and Vibration 456 (2019) 137–161. ISSN: 0022-460X
[28] D. Yang, D. Laera, A.S. Morgans, Open source combustion instability low order simulator for annular combustors (OSCILOS_ann).
[29] J. Li, D. Yang, C. Luzzato, A.S. Morgans, Open source combustion instability low order simulator (OSCILOS-long) technical report.
[30] S.M. Camporeale, B. Fortunato, G. Campa, A finite element method for three-dimensional analysis of thermo-acoustic combustion instability, J. Eng. Gas Turbine Power 133 (1) (2011) 011506, doi:10.1115/1.4000606.
[31] F. Nicoud, L. Benoit, C. Sensiau, T. Poinsot, Acoustic modes in combustors with complex impedances and multidimensional active flames, AIAA J. 45 (2) (2007) 426–441.
[32] C.F. Silva, F. Nicoud, T. Schuller, D. Durox, S. Candel, Combining a Helmholtz solver with the flame describing function to assess combustion instability in a premixed swirled combustor, Combust. Flame 160 (9) (2013) 1743–1754.
[33] F. Ni, M. Miguel-Brebion, F. Nicoud, T. Poinsot, Accounting for acoustic damping in a Helmholtz solver, AIAA J. 55 (4) (2017) 1205–1220.
[34] X. Han, A.S. Morgans, Non-linear interactions of two premixed flames explored by large eddy simulation with external acoustic forcing, Combust. Sci. Technol. 190 (3) (2018) 425–436.
[35] J. Li, Y. Xia, A.S. Morgans, X. Han, Numerical prediction of combustion instability limit cycle oscillations for a combustor with a long flame, Combust. Flame 185 (2017) 28–43.
[36] F.E. Marble, S.M. Candel, Acoustic disturbance from gas non-uniformities convected through a nozzle, J. Sound Vib. 55 (2) (1977) 225–243.
[37] N.A. Eisenberg, T.W. Kao, Propagation of sound through a variable-area duct with a steady compressible flow, J. Acoust. Soc. Am. 49 (1B) (1971) 169–175.
[38] V. Easwaran, M.L. Munjal, Plane wave analysis of conical and exponential pipes with incompressible mean flow, J. Sound Vib. 152 (1) (1992) 73–93.
[39] M.L. Munjal, M.G. Prasad, On plane-wave propagation in a uniform pipe in the presence of a mean flow and a temperature gradient, J. Acoust. Soc. Am. 80 (5) (1986) 1501–1506.

[40] R.I. Sujith, G.A. Waldherr, B.T. Zinn, An exact solution for one-dimensional acoustic fields in ducts with an axial temperature gradient, J. Sound Vib. 184 (3) (1995) 389–402.
[41] B. Karthik, B.M. Kumar, R.I. Sujith, Exact solutions to one-dimensional acoustic fields with temperature gradient and mean flow, J. Acoust. Soc. Am. 108 (1) (2000) 38–43.
[42] P.B. Subrahmanyam, R.I. Sujith, T.C. Lieuwen, A family of exact transient solutions for acoustic wave propagation in inhomogeneous, non-uniform area ducts, J. Sound Vib. 240 (4) (2001) 705–715.
[43] A. Schlissel, The initial development of the WKB solutions of linear second order ordinary differential equations and their use in the connection problem, Hist. Math. 4 (2) (1977) 183–204.
[44] A. Cummings, Ducts with axial temperature gradients: an approximate solution for sound transmission and generation, J. Sound Vib. 51 (1) (1977) 55–67.
[45] J. Li, A.S. Morgans, The one-dimensional acoustic field in a duct with arbitrary mean axial temperature gradient and mean flow, J. Sound Vib. 400 (2017) 248–269.
[46] E. Dokumaci, An approximate analytical solution for plane sound wave transmission in inhomogeneous ducts, J. Sound Vib. 217 (5) (1998) 853–867.
[47] E. Dokumaci, Comment on "the one dimensional acoustic field with arbitrary mean axial temperature gradient and mean flow", J. Li and AS Morgans, Journal of Sound and Vibration 400 (2017) 248–269) 410 (2017) 485–487.
[48] V.K. Rani, S.L. Rani, WKB solutions to the quasi 1-D acoustic wave equation in ducts with non-uniform cross-section and inhomogeneous mean flow properties-acoustic field and combustion instability, J. Sound Vib. 436 (2018) 183–219.
[49] O.M. Umurhan, Exploration of Fundamental Matters of Acoustic Instabilities in Combustion Chambers, Center for Turbulence Research Annual Briefs, 1999, pp. 85–98.
[50] E. Dokumaci, On transmission of sound in a non-uniform duct carrying a subsonic compressible flow, J. Sound Vib. 210 (3) (1998) 391–401.
[51] I. Duran, S. Moreau, Solution of the quasi-one-dimensional linearized euler equations using flow invariants and the magnus expansion, J. Fluid Mech. 723 (2013) 190–231.
[52] J. Li, D. Yang, A.S. Morgans, The effect of an axial mean temperature gradient on communication between one-dimensional acoustic and entropy waves, Int. J. Spray Combust. Dyn. 10 (2) (2018) 131–153.
[53] A.S. Morgans, C.S. Goh, J.A. Dahan, The dissipation and shear dispersion of entropy waves in combustor thermoacoustics, J. Fluid Mech. (2013) 733.
[54] Y. Xia, I. Duran, A.S. Morgans, X. Han, Dispersion of entropy perturbations transporting through an industrial gas turbine combustor, Flow Turbul. Combust. 100 (2) (2018) 481–502.
[55] A.P. Dowling, S. Hubbard, Instability in lean premixed combustors, Proc. Inst. Mech. Eng. Part A 214 (4) (2000) 317–332.
[56] T. Sattelmayer, Influence of the combustor aerodynamics on combustion instabilities from equivalence ratio fluctuations, J. Eng. Gas Turbines Power 125 (1) (2003) 11–19.
[57] U. Ingard, V.K. Singhal, Upstream and downstream sound radiation into a moving fluid, J. Acoust. Soc. Am. 54 (5) (1973) 1343–1346.
[58] P. Palies, D. Durox, T. Schuller, S. Candel, Nonlinear combustion instability analysis based on the flame describing function applied to turbulent premixed swirling flames, Combust. Flame 158 (10) (2011) 1980–1991.
[59] T.C. Lieuwen, Unsteady Combustor Physics, Cambridge University Press, 2012 Aug 27.
[60] S.W. Rienstra, A. Hirschberg, An introduction to acoustics, Eindhoven Univ. Technol. 18 (2004) 19.
[61] A.P. Dowling, Y. Mahmoudi, Combustion noise, Proc. Combust. Inst. 35 (1) (2015) 65–100.